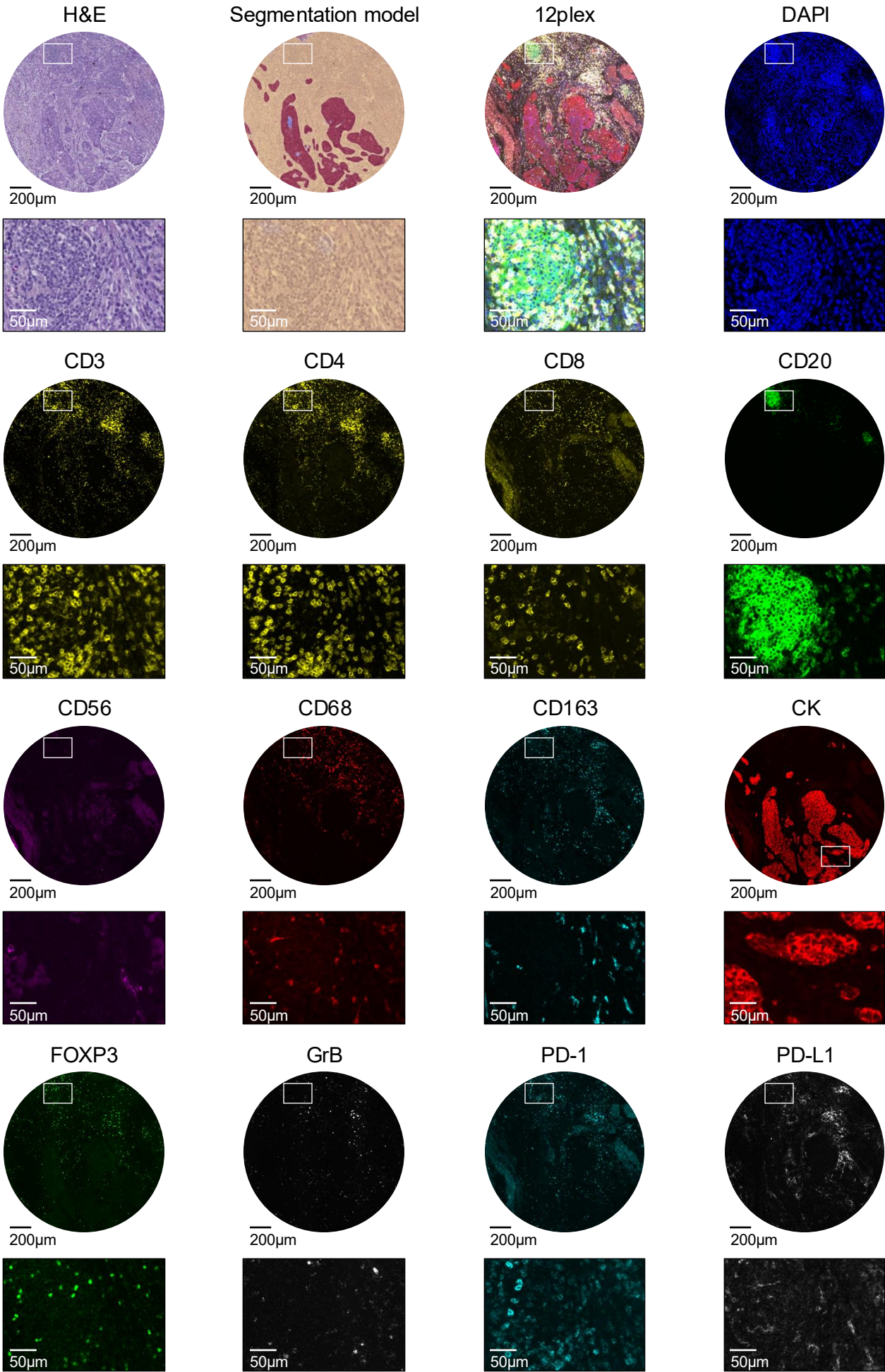
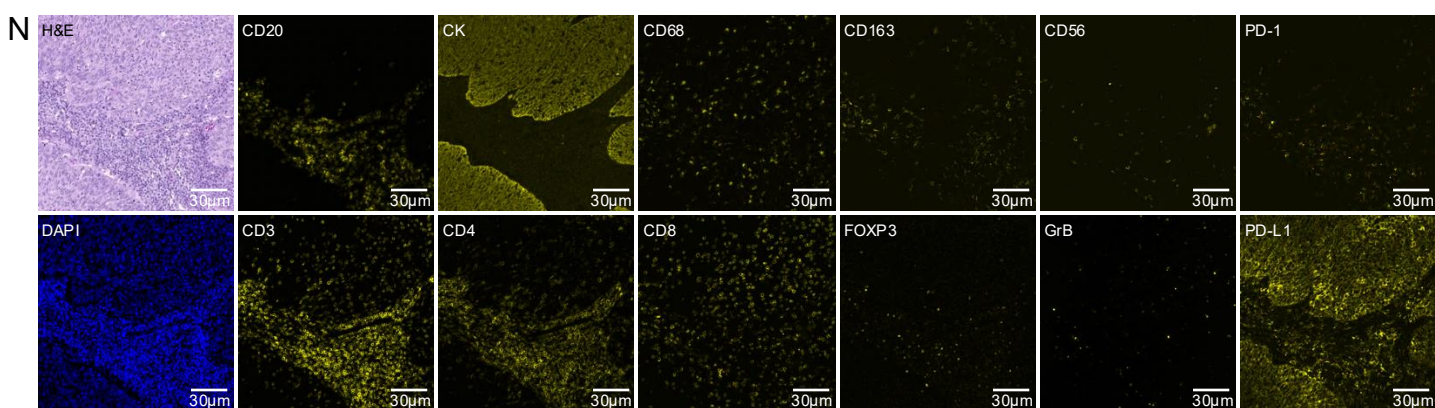
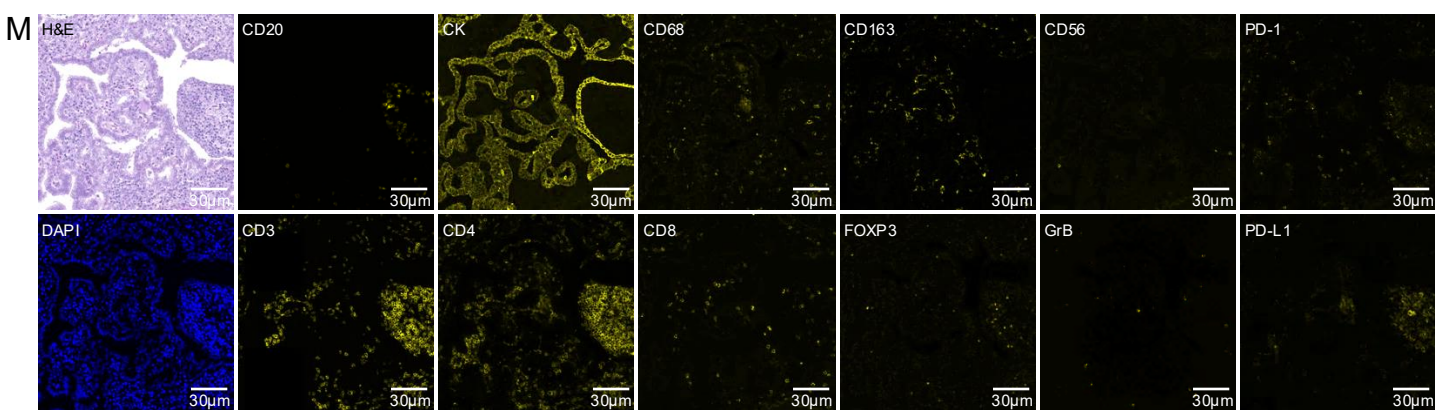
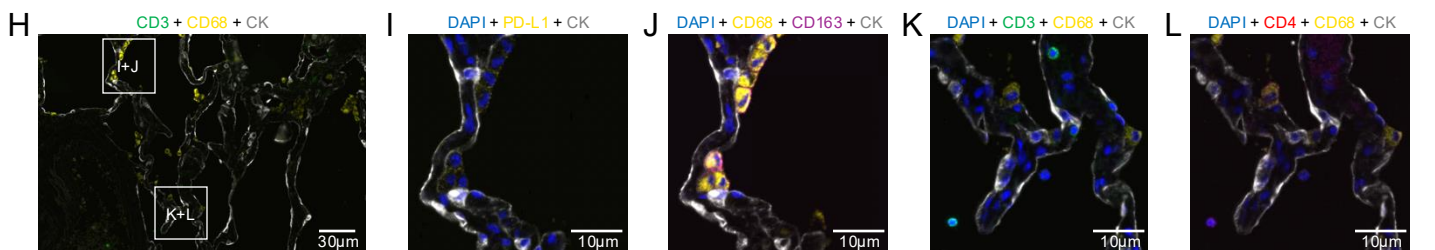
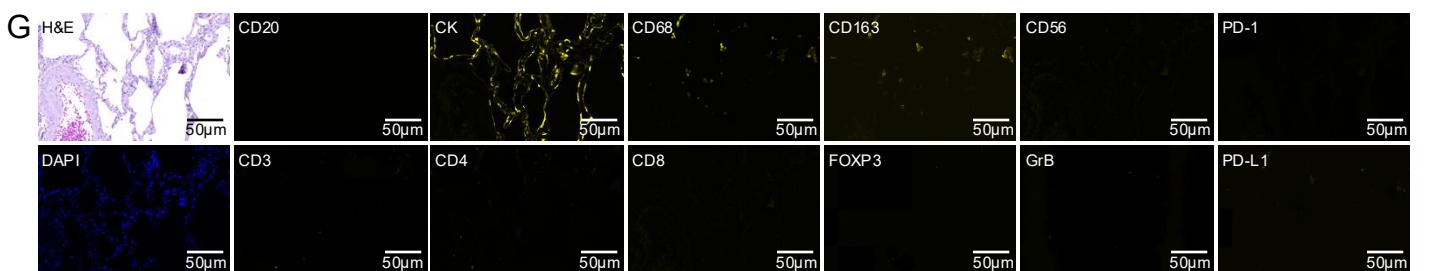
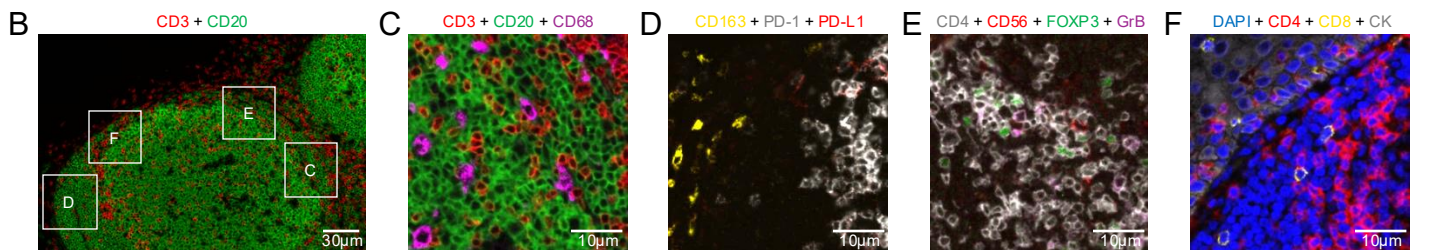
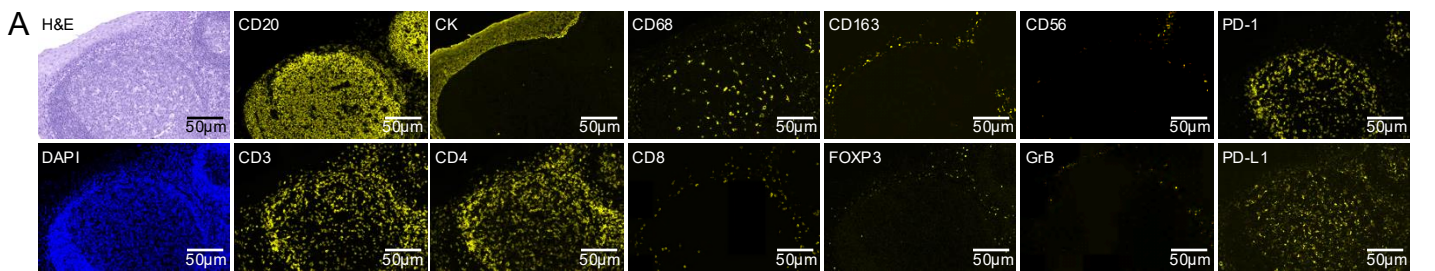


Supplementary Information



Supplementary Figure 1: Overview of imaging data modalities and markers.

Each of the four rows shows different image modalities and marker views of the same representative tumor sample ($n = 1$), with whole tissue spots in the upper panel and its respective magnified views directly below. From left to right in the top row: H&E staining, tissue segmentation model heatmap, the combined 12-plex mIF panel, and the DAPI channel (blue). The second row shows CD3, CD4, and CD8 (all in yellow) and CD20 (green). The third-row displays CD56 (magenta), CD68 (red), CD163 (cyan-blue), and CK (red). The fourth row shows FOXP3 (green), GrB (white), PD-1 (cyan-blue), and PD-L1 (white). Images are read from left to right in each row. Scale bars: 200 μ m (tissue spots) and 50 μ m (magnified regions).



Supplementary Figure 2: Marker validation.

(A) Validation of markers on lymphatic tissue (n = 1 tissue sample): The tonsil tissue shows the expected staining patterns for all applied markers.

(B-F) Staining overlays of tonsil tissue (n = 1 tissue sample) demonstrate the expected patterns of histologic architecture, subcellular structures (nucleus, cytoplasm, membrane), and protein co-expression.

(G) Validation of the assay on lung tissue (n = 1 tissue sample) : Lung tissue shows the expected staining patterns for all applied markers. Staining artifacts, which are frequently observed in erythrocytes (bottom left) and within the alveolar spaces, are not visible.

(H-L) Staining overlays of lung tissue (n = 1 tissue sample) illustrate the expected patterns of histologic architecture, subcellular structures (nucleus, cytoplasm, membrane), and protein co-expression.

(M+N) Representative staining of one LUAD (n = 1 tumor sample; M) and one LUSC patient (n = 1 tumor sample; N).

Scale bars: (A+G) 50µm, (B+H+M+N) 30µm, (C-F+I-L) 10µm

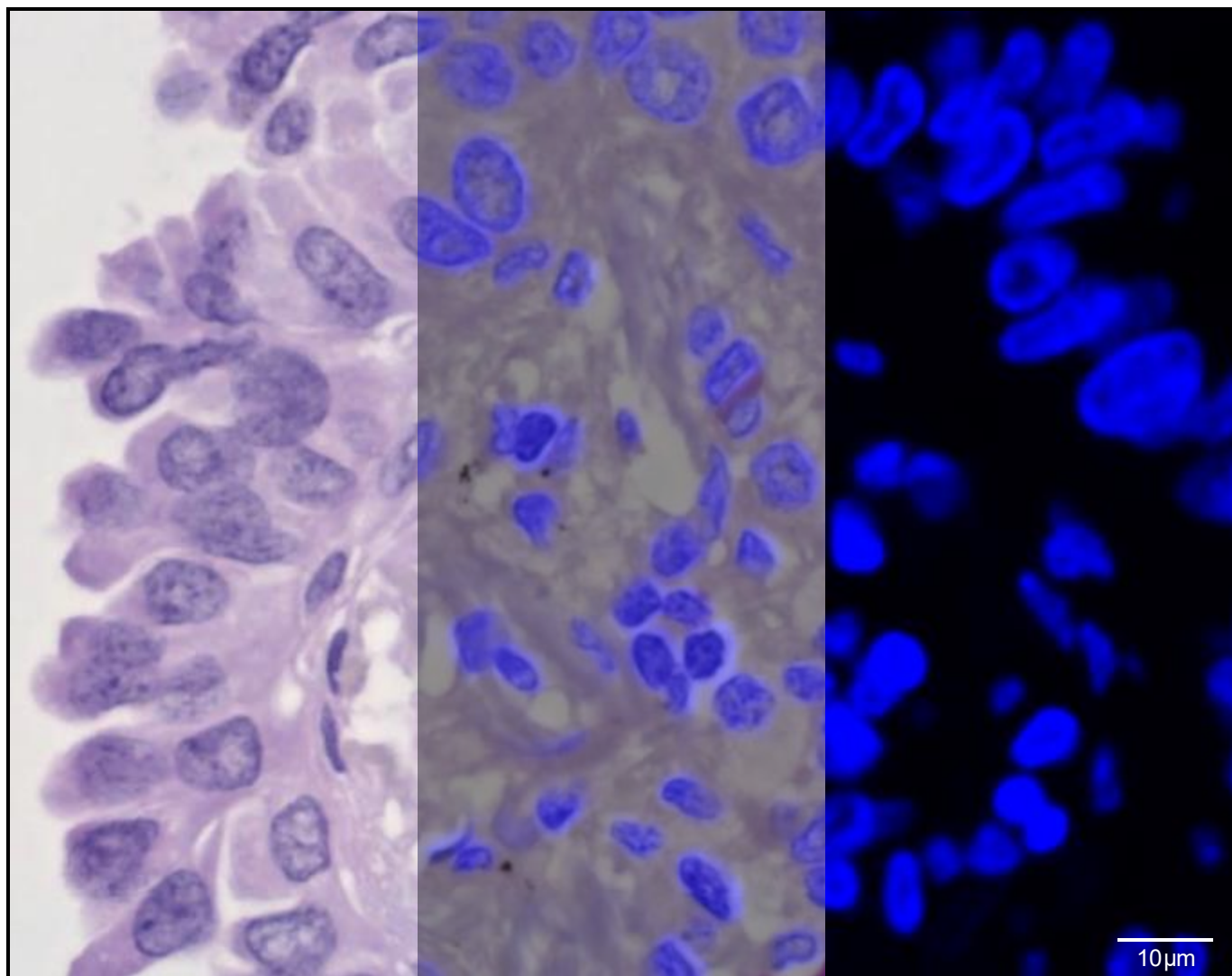
T cell									
	H&E	mIF	DAPI	CD3	CD4	CD8	FOXP3	CD56	
CD3T									
Th									
CD8T									
DPT									
Treg									
Cytotoxic									
	H&E	mIF	DAPI	CD3	CD4	CD8	GrB		
cCD3T									
cCD4T									
cCD8T									
cDPT									
Activated									
	H&E	mIF	DAPI	CD3	CD4	CD8	FOXP3	PD-1	GrB
acCD3T									
acCD4T									
acCD8T									
acDPT									
aTreg									
Exhausted									
	H&E	mIF	DAPI	CD3	CD4	CD8	FOXP3	CD56	PD-1
exCD3T									
exCD3T56									
exTh									
exCD8T									
exDPT									
exTreg									
Imm.sup.									
	H&E	mIF	DAPI	CD3	CD4	CD8	CD56	PD-L1	
iCD3T									
iCD4T									
iCD8T									
iDPT									

Cancer							
	H&E	mIF	DAPI	CK	CD56		
CC							
CC56							
Imm.sup.							
	H&E	mIF	DAPI	CK	CD56	PD-L1	
iCC							
iCC56							
B cell							
	H&E	mIF	DAPI	CD20			
B							
Activated							
	H&E	mIF	DAPI	CD20	PD-1		
aB							
Imm.sup.							
	H&E	mIF	DAPI	CD20	PD-L1		
iB							
NK cell							
	H&E	mIF	DAPI	CD56	CD8	GrB	
NKbr							
NKdim							
Activated							
	H&E	mIF	DAPI	CD56	GrB	PD-1	
aNK							
Imm.sup.							
	H&E	mIF	DAPI	CD56	PD-L1		
iNK							
Mφ							
	H&E	mIF	DAPI	CD68	CD163	PD-1	
M1							
M2							
M1_PD1+							
M2_PD1+							
Imm.sup.							
	H&E	mIF	DAPI	CD68	CD163	PD-1	PD-L1
iM1							
iM2							
iM1_PD1+							
iM2_PD1+							

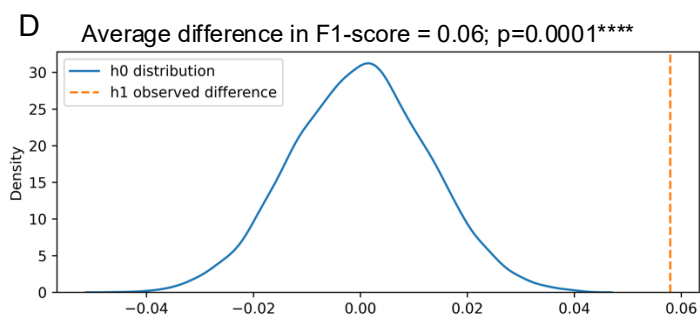
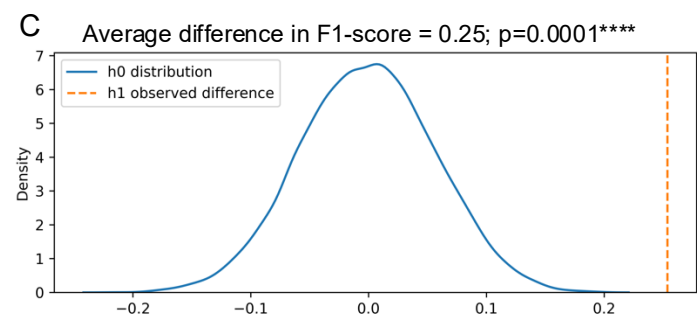
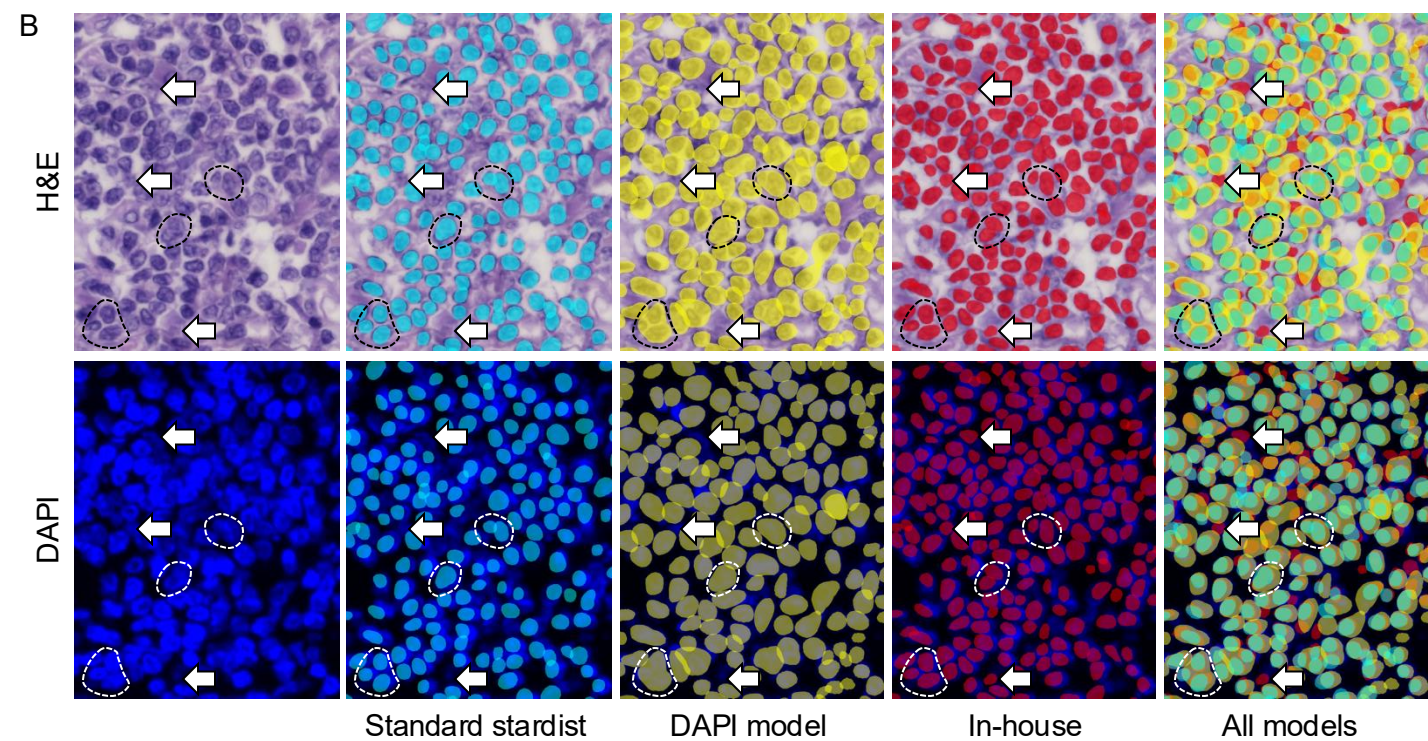
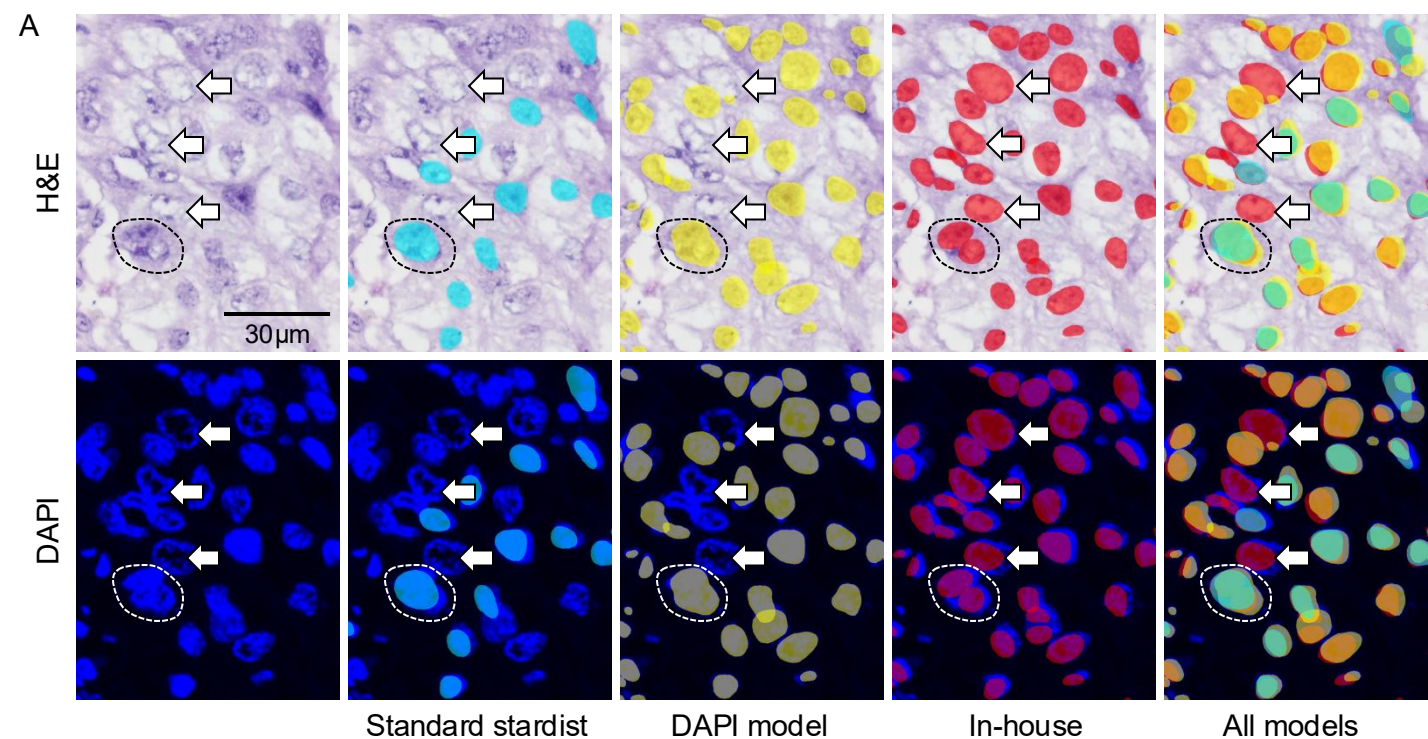
Supplementary Figure 3: Marker expression across all 43 cell phenotypes.

Cell phenotypes are shown for one representative tumor sample (n = 1), classified according to their primary cell type and subsequently subdivided based on their cellular status (cytotoxic, activated, exhausted, immunosuppressive). T cells are indicated by green, carcinoma cells by red, B cells by yellow, NK cells by purple and macrophages by cyan. Figure shows cell phenotype name abbreviations. For full names see Supplementary Table 2.

Scale: each image represents a 15 µm field of view.



Supplementary Figure 4: Co-registration of H&E and mIF data.
Center image showing precise alignment of H&E-stain (left) and mIF (DAPI) stain (right; n = 1 tumor sample).
Scale bar: 10µm



Supplementary Figure 5: Comparative analysis of cell detection models.

Standard StarDist model (cyan; F1-score=0.682), standard DAPI model (yellow; F1-score=0.855) compared to our optimized StarDist model (red; F1-score=0.913).

(A) The standard models are less sensitive (recall) and miss to detect cells that our optimized version does cover (exemplary cells are indicated by white arrows; n = 1 tumor sample). In comparison to our optimized model, individual cells are less well discriminated by the standard models (two exemplary cells framed by white dashed lines are detected as a single cell by the standard models).

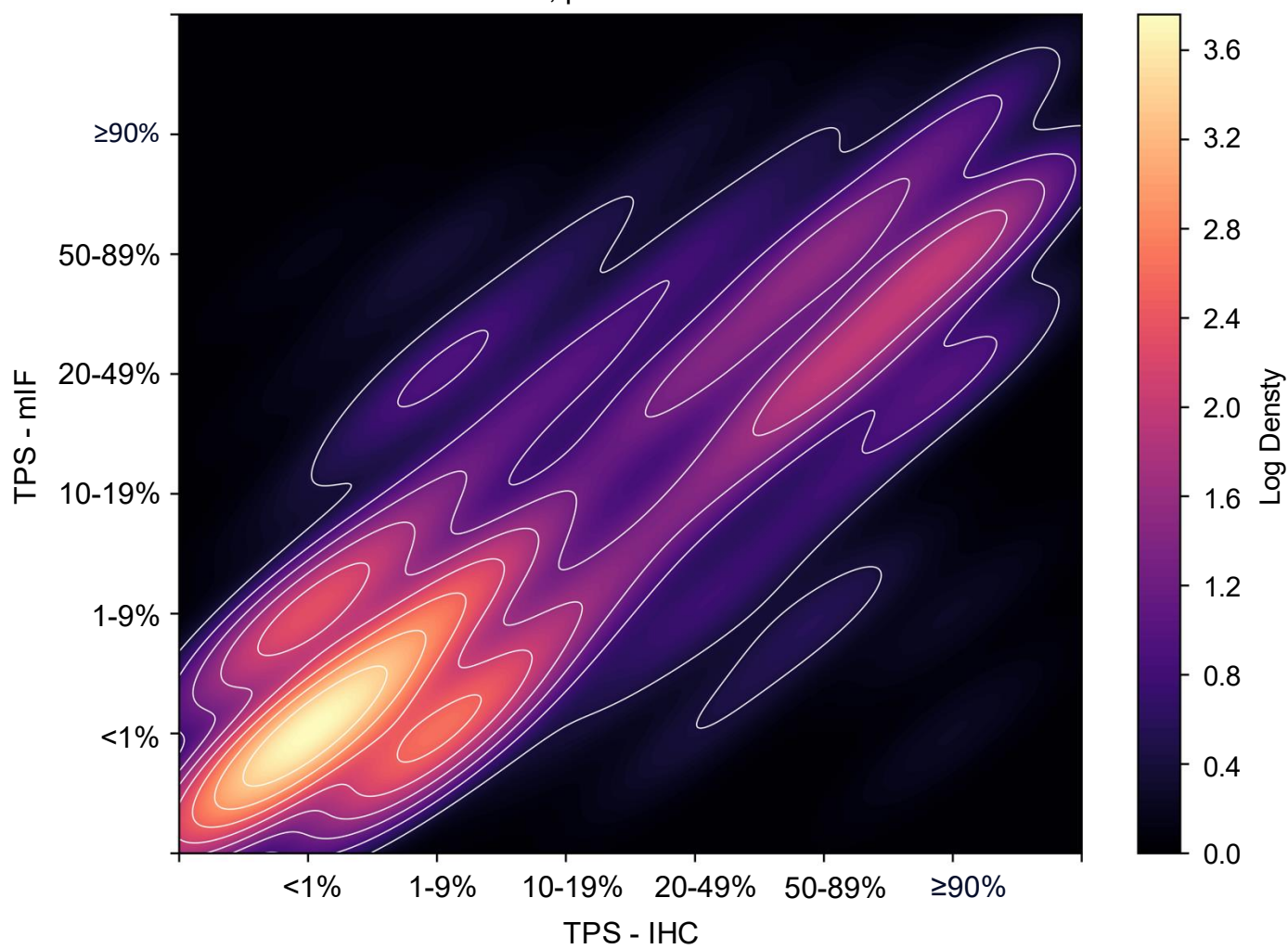
(B) Similar observations can be made within tissue areas of high cellularity (n = 1 tumor sample). In particular, the DAPI model often does not discriminate well between individual cells (exemplary cells framed by white dashed lines).

(C) The performance of the In-house model is compared to the Standard StarDist (H&E) model and tested for statistical significance using a permutation test over the per slide F1 scores.

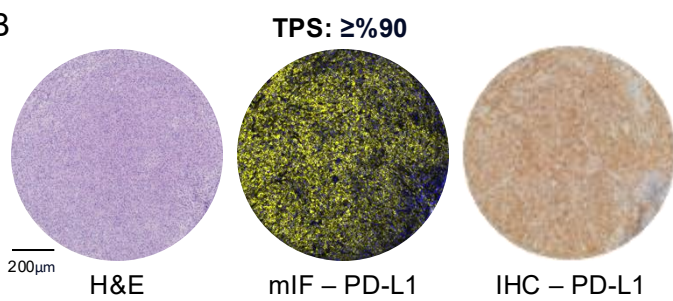
(D) Same as (C) but for comparison of In-house and the DAPI model.

Scale bars: (A+B) 30µm

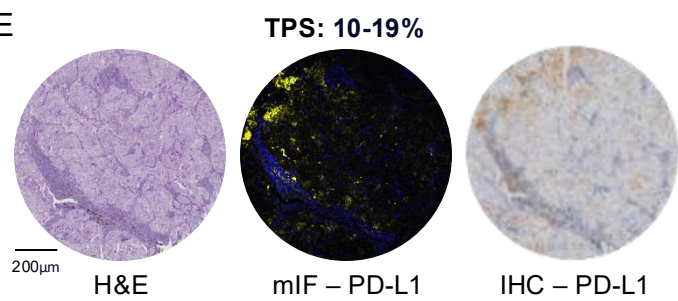
A

 $r = 0.8413$; $p\text{-value} = 3.083\text{E-}209$ 

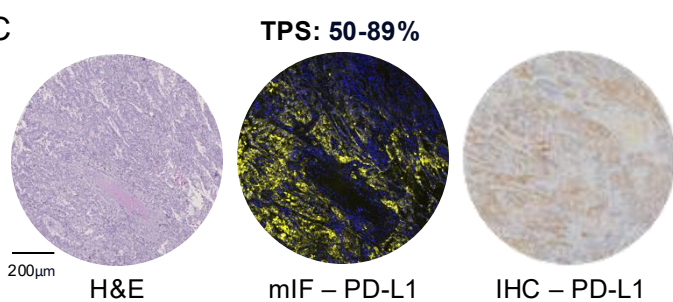
B



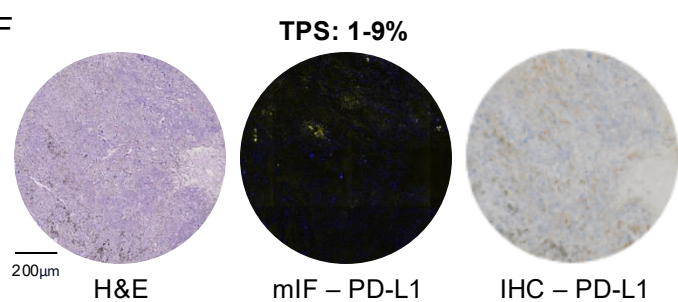
E



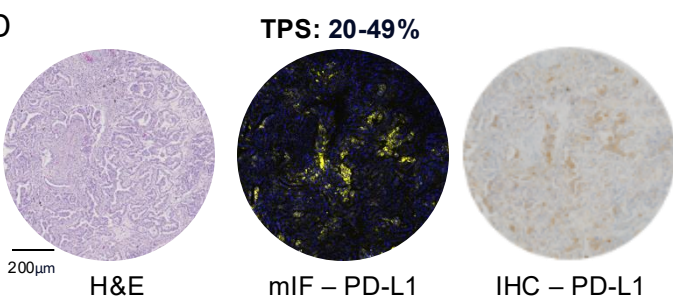
C



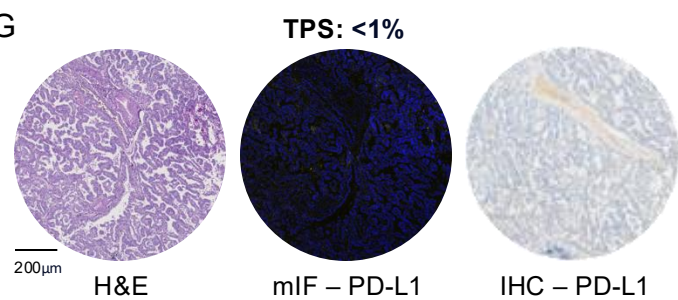
F



D



G

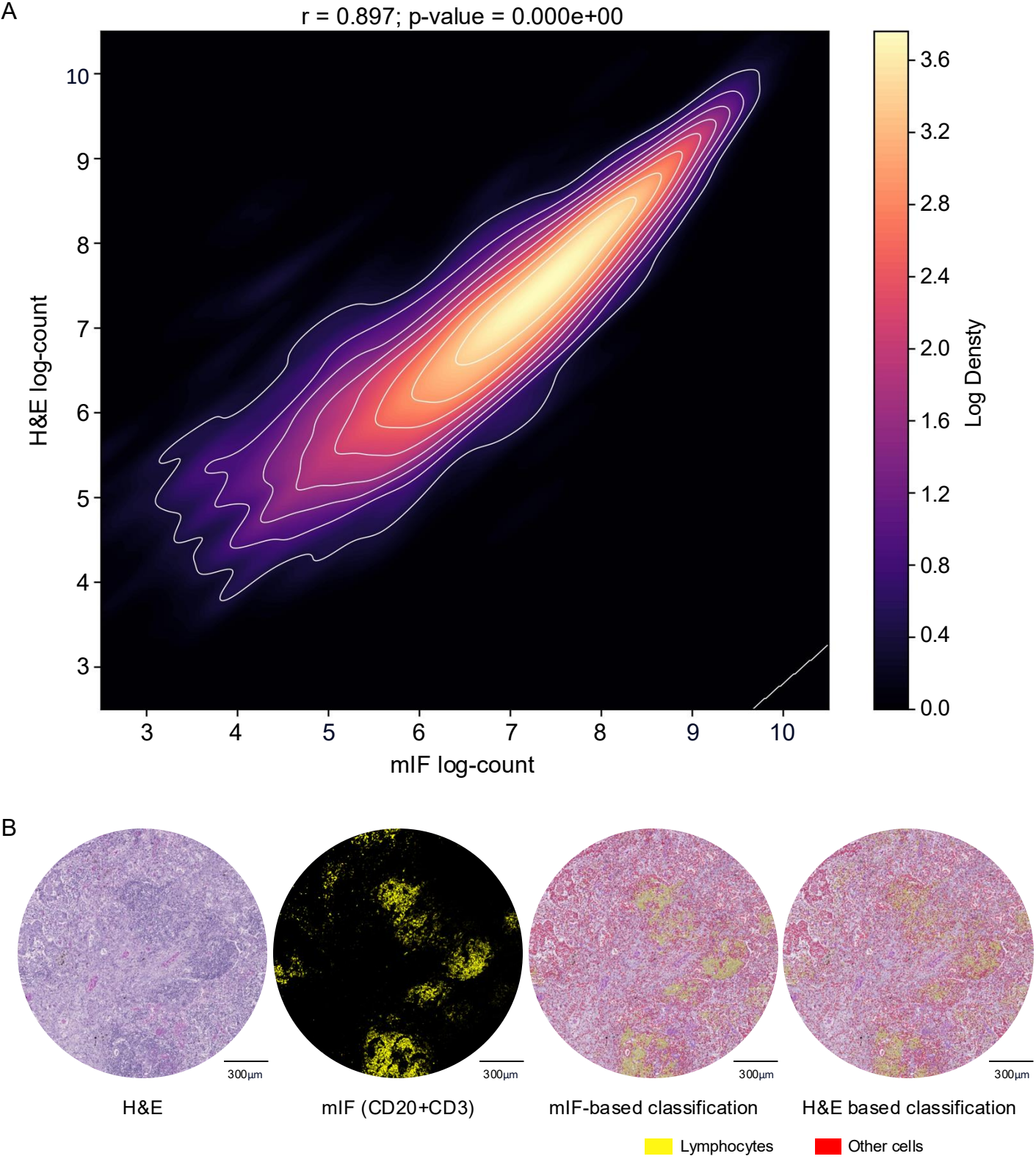


Supplementary Figure 6: Validation of the tumor proportion score (TPS) by IHC.

(A) Correlation of the TPS evaluation through automated analysis of mIF staining (y-axis), with the evaluation through the pathologist of IHC staining (x-axis). Statistical significance was assessed using Pearson's correlation (`scipy.stats.pearsonr`; $n = 769$ patients).

(B-G) Examples of tumors with different TPS ranges, stained by H&E (left), mIF (center) and IHC (right). Colors in mIF: Blue = DAPI, yellow = PD-L1.

Scale bars: (B-G) 200 μ m

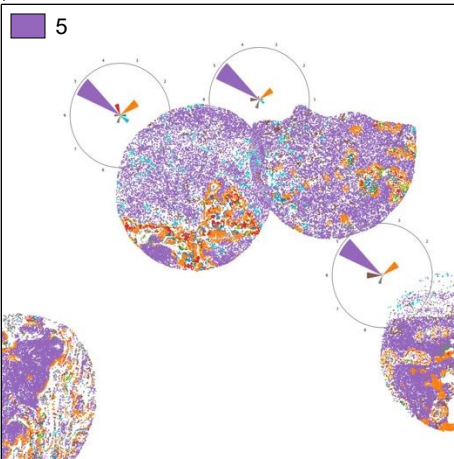
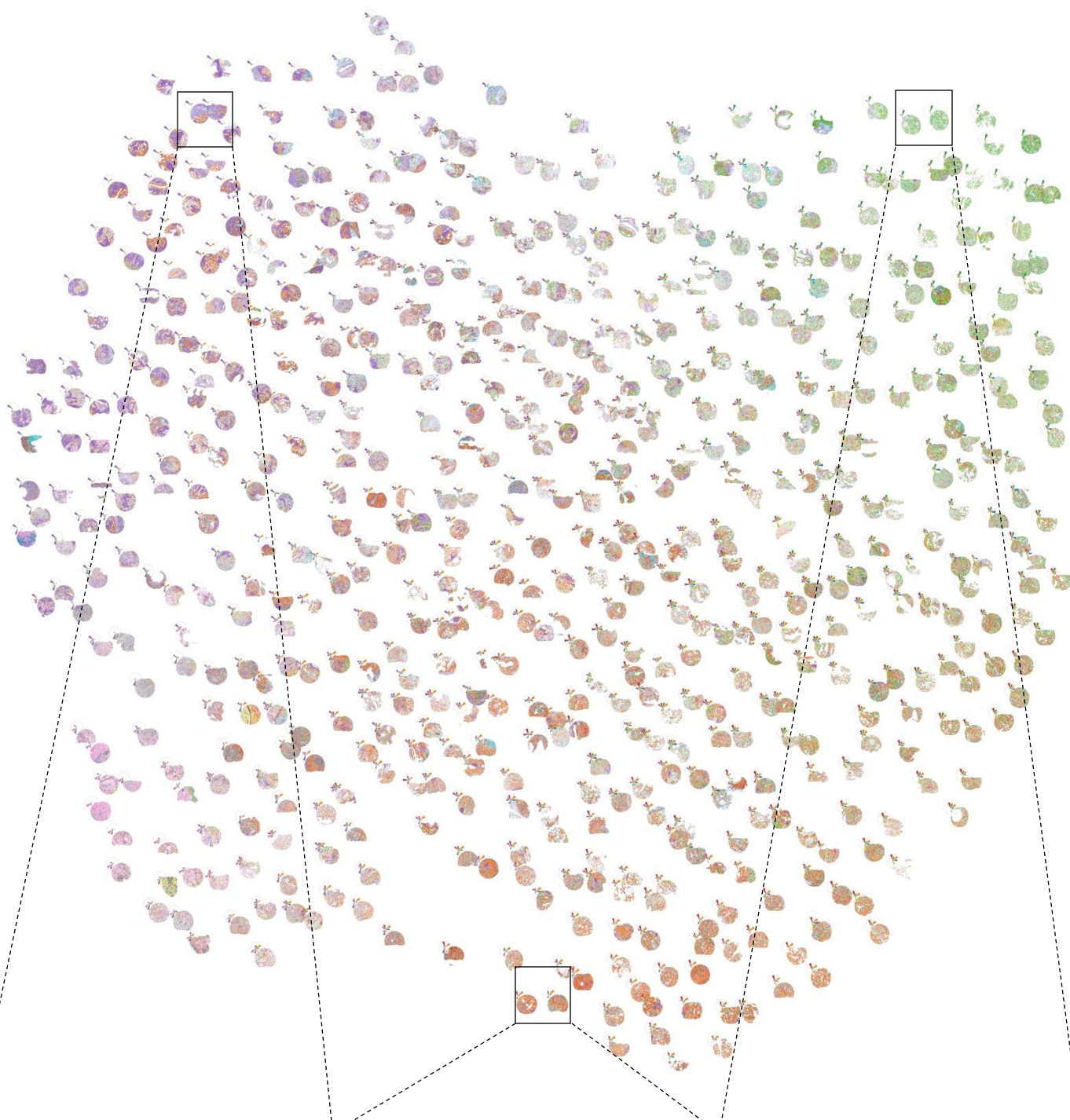


Supplementary Figure 7: Validation of the lymphocyte counts by H&E-based cell classification.

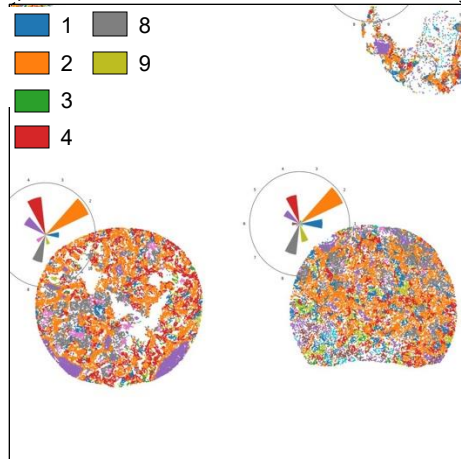
(A) Correlation of the lymphocytes counts detected by H&E-based cell classification (y-axis), with detection by mIF-based cell classification (x-axis). Statistical significance was assessed using Pearson's correlation (scipy.stats.pearsonr; $n = 3807$ tumor samples from 1125 patients).

(B) Exemplary tissue core stained by H&E (left), stained by mIF (center left), with AI-derived mIF-based cell classification (center right) and AI-derived H&E-based cell classification (right). Colors in mIF: Yellow = CD3+CD20.

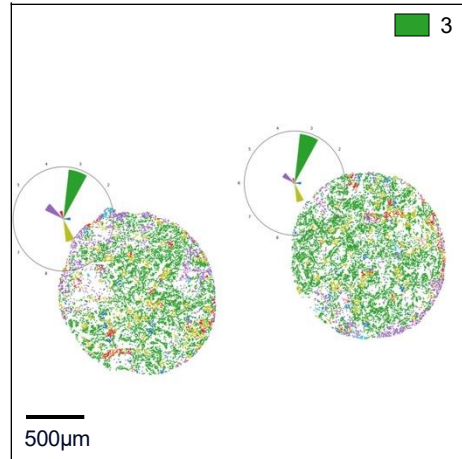
Scale bars: (B) 300µm



I



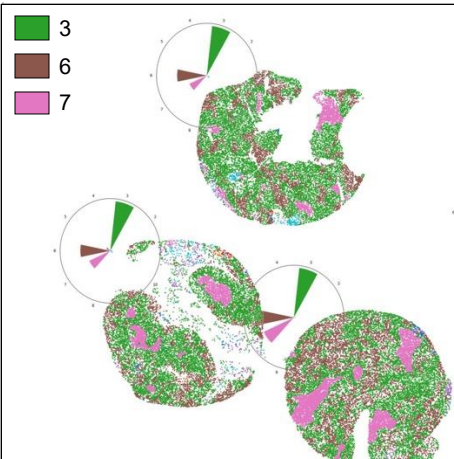
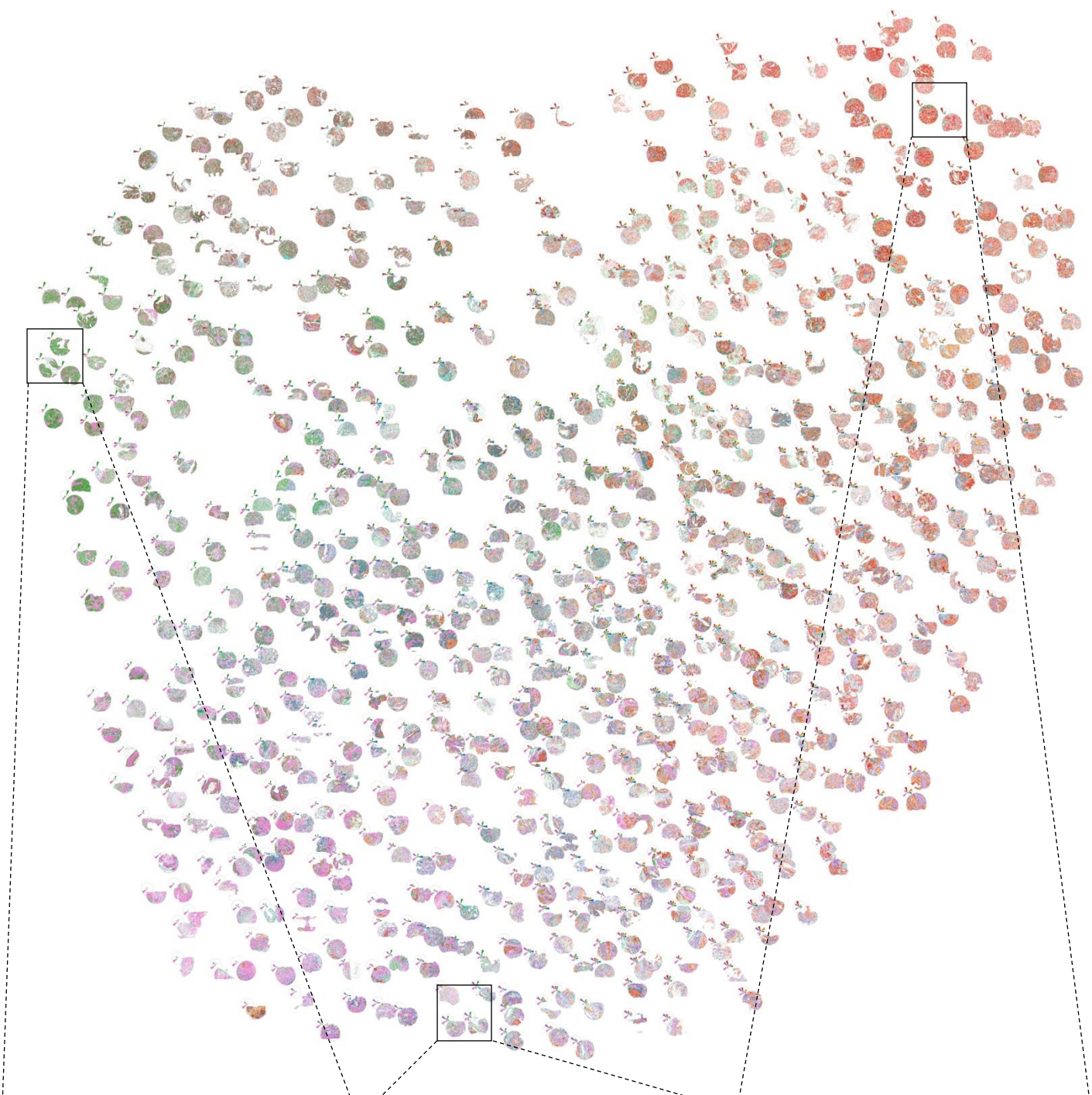
II



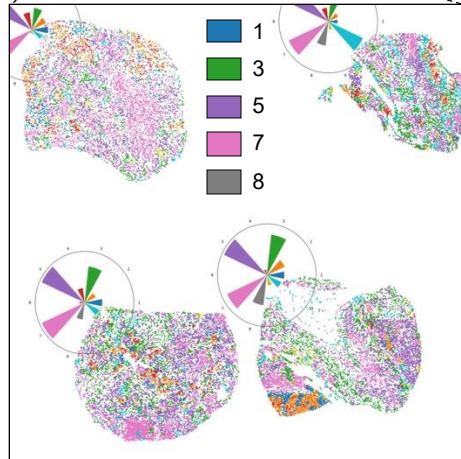
III

Supplementary Figure 8: LUAD niche atlas for all tumor samples (magnified version).

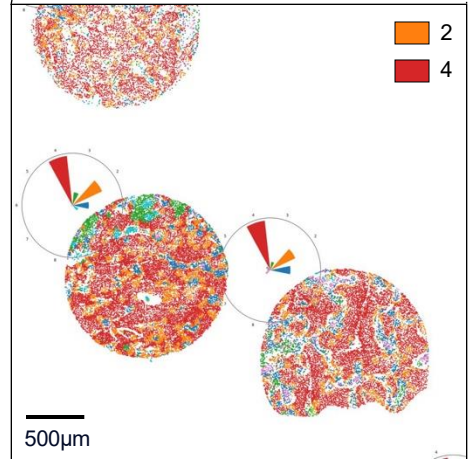
UMAP projection of n = 2,233 tumor samples according to niche patterns shows distinct groups (I, II, III; scale bar: 500μm). Each dot on tumor samples corresponds to a single cell, and colors indicate the assigned cellular niche.



I



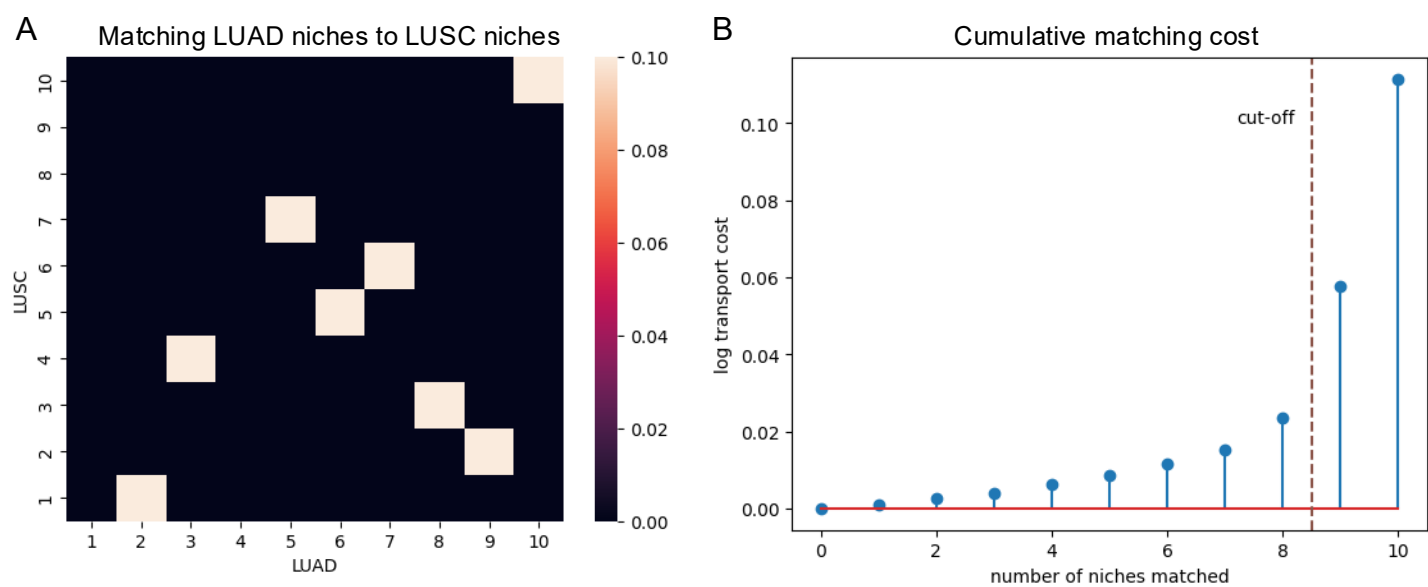
II



III

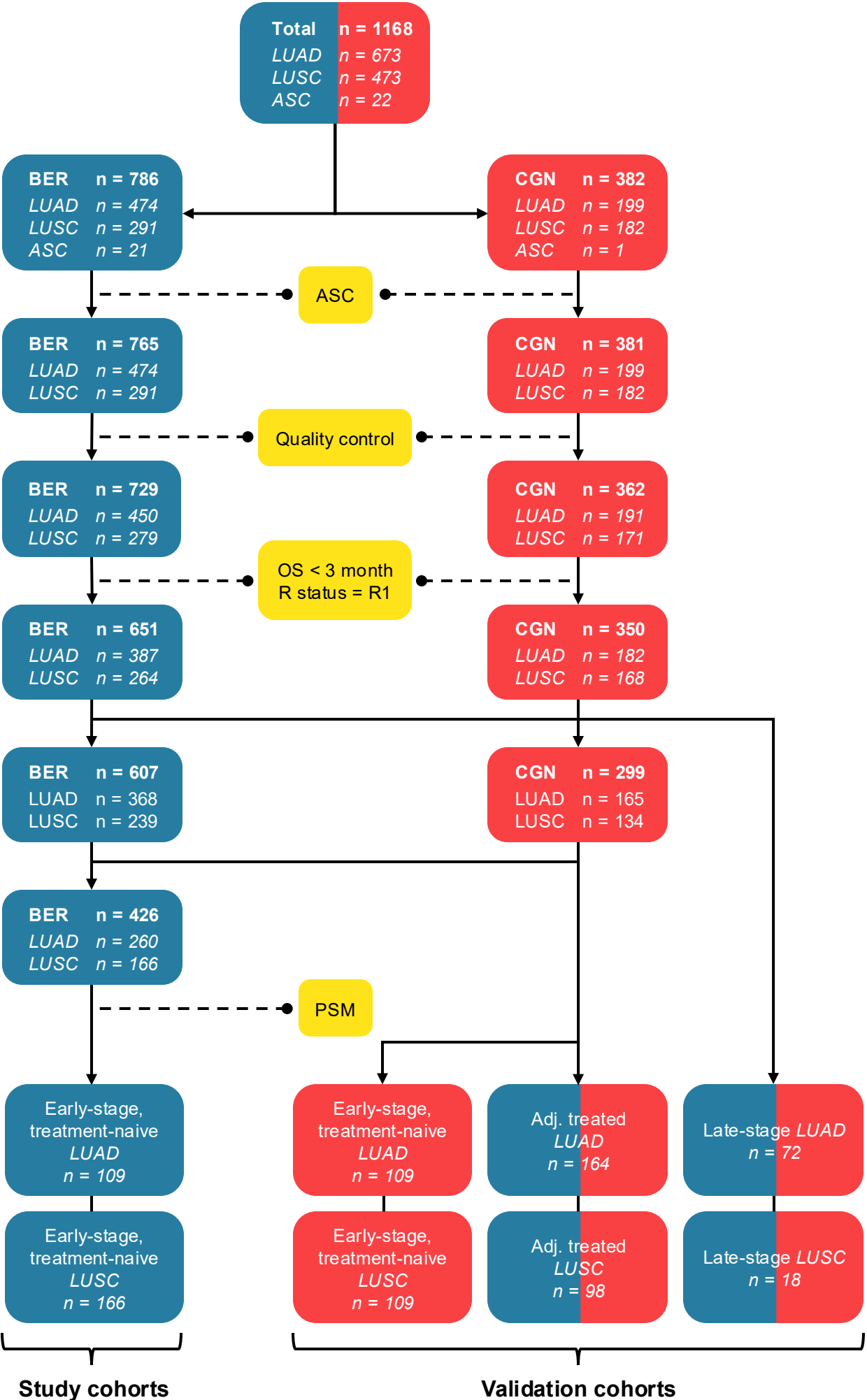
Supplementary Figure 9: LUSC niche atlas for all tumor samples (magnified version).

UMAP projection of n = 1,659 tumor samples according to niche patterns shows distinct groups (I, II, III; scale bar: 500μm). Each dot on tumor samples corresponds to a single cell, and colors indicate the assigned cellular niche.



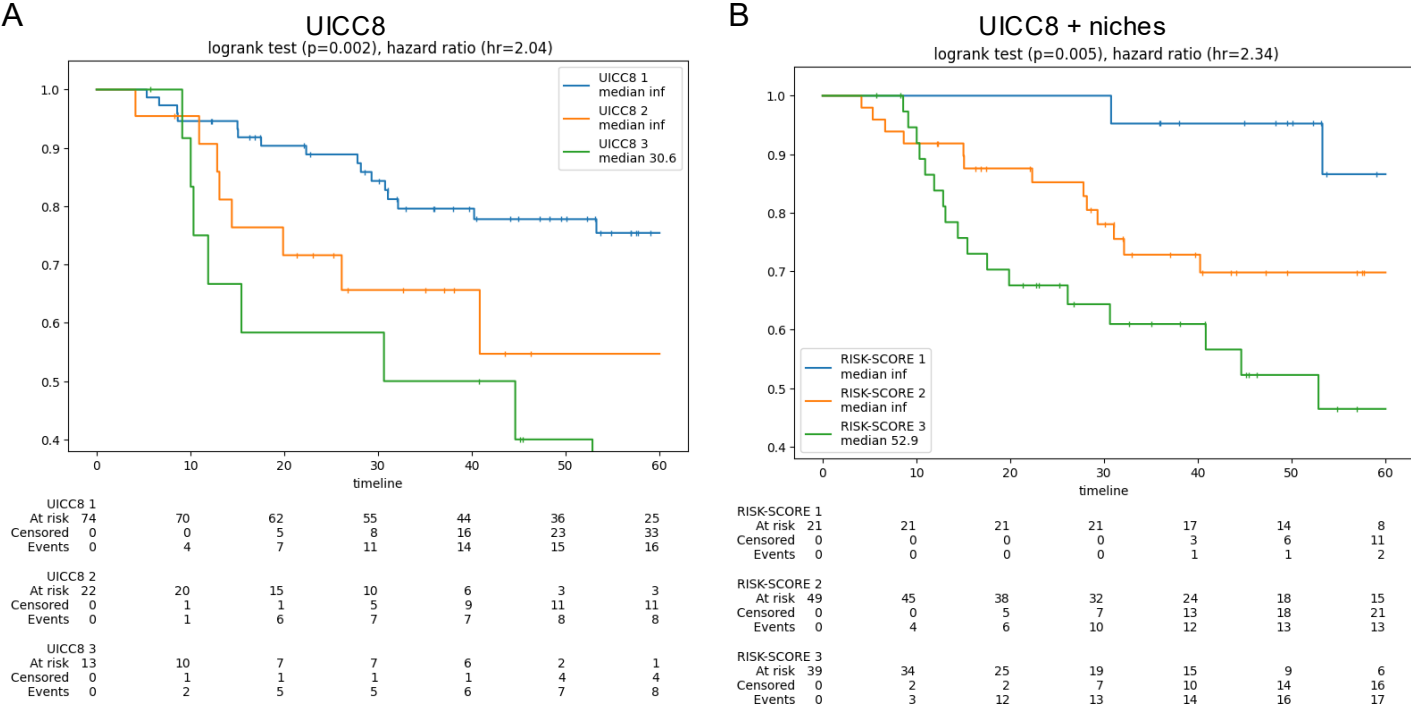
Supplementary Figure 10: Comparison of LUAD and LUSC niches.

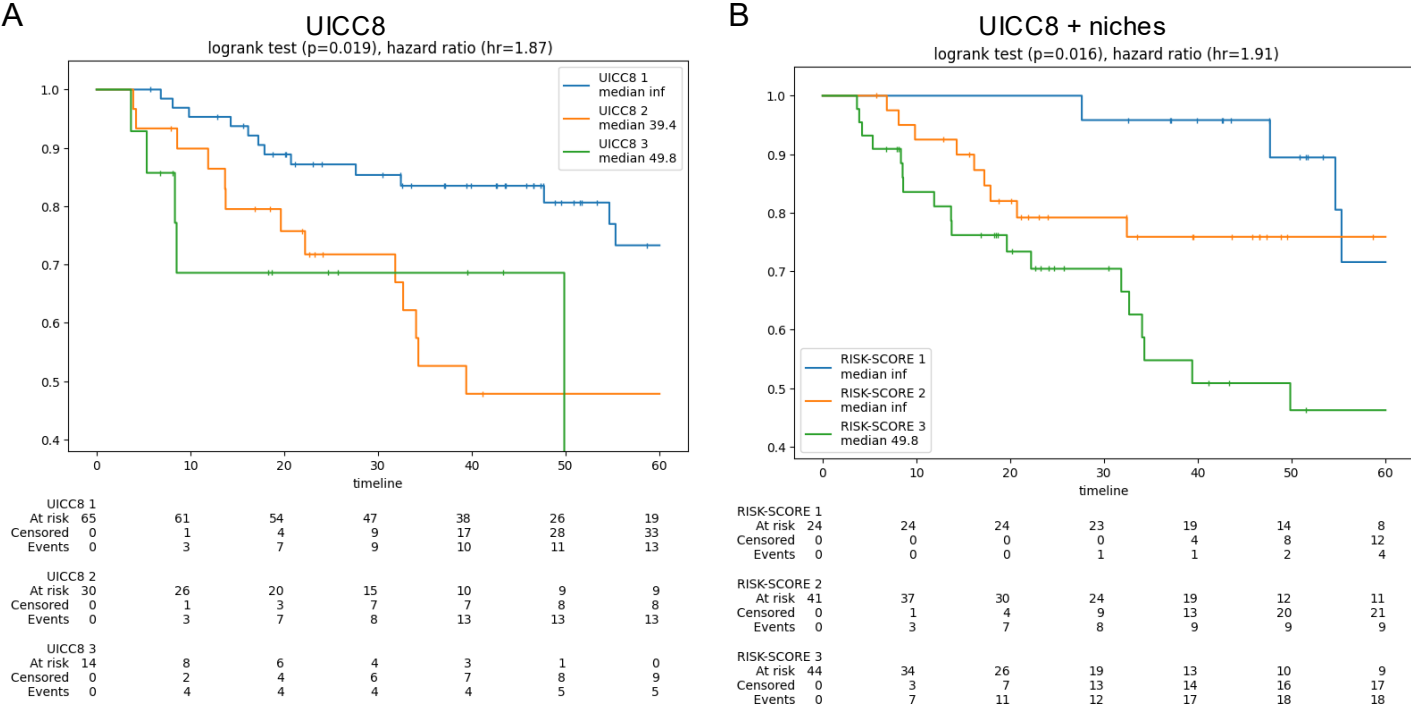
(A) We find similarities among the cell niches in LUAD and LUSC in terms of their distribution of contained phenotypes. To suggest a 1:1 matching, we adapt the partial Wasserstein optimal transport formulation with a chi-square-metric and present the solution for an 80% match. (B) We stop the matching process at 80% to avoid excessively high transport costs that appear on the 9th and 10th matches.

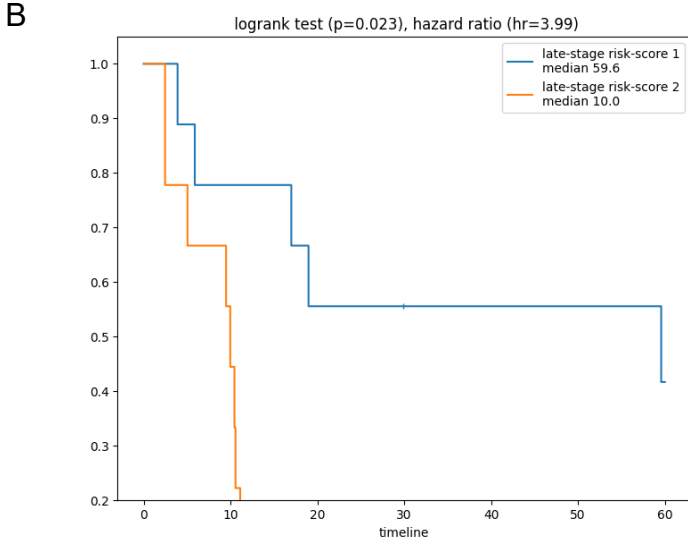
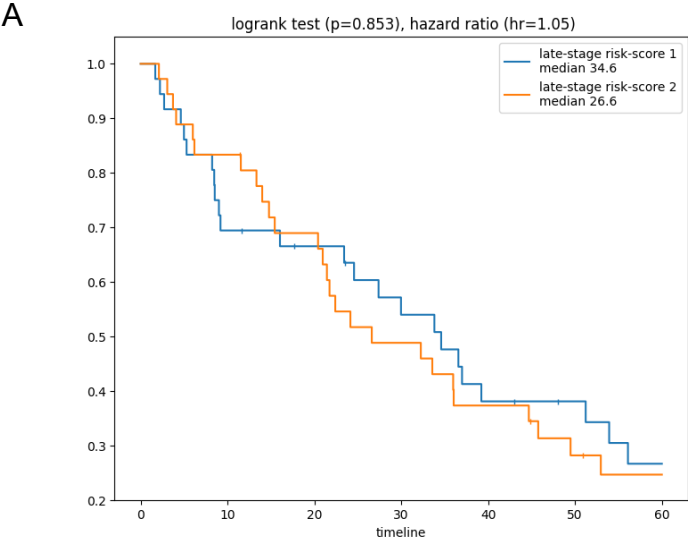


Supplementary Figure 11: Detailed patient selection flowchart.

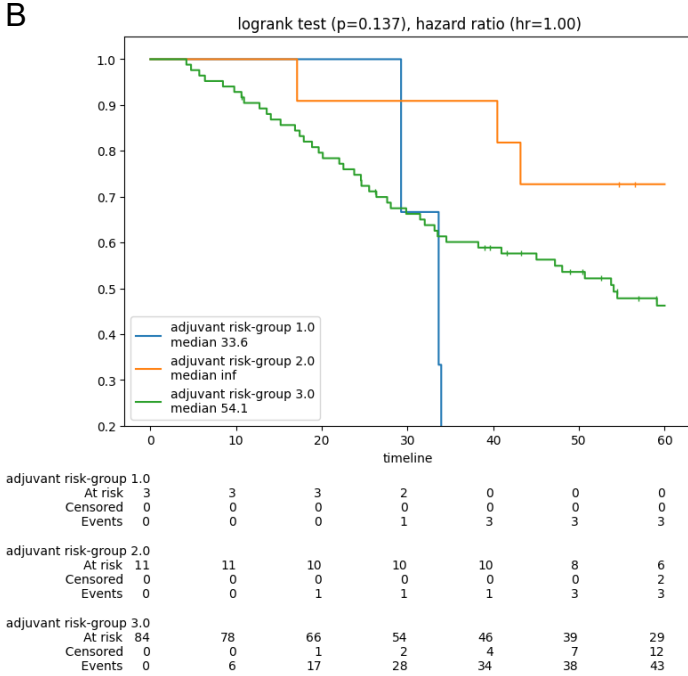
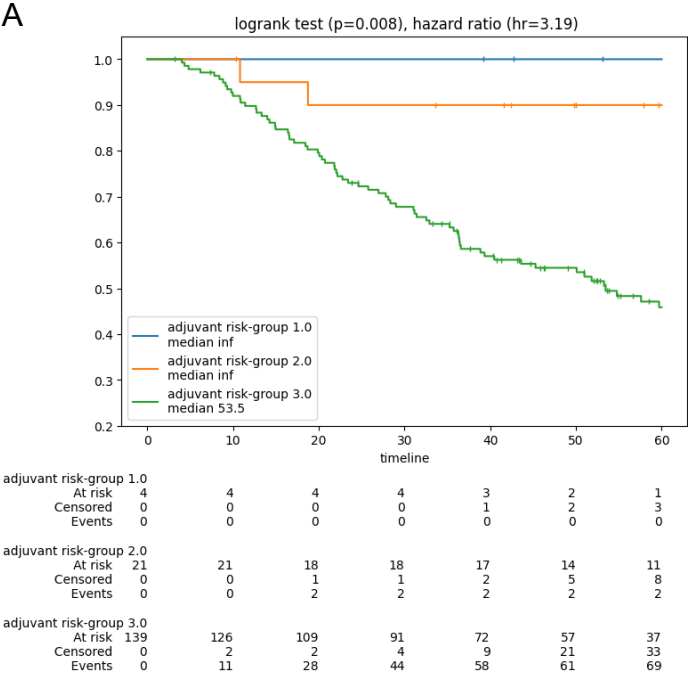
The patients from Berlin and Cologne are indicated by blue and red, respectively, while exclusion criteria are highlighted in yellow. ASC (adenosquamous carcinoma), OS (overall survival), R status (resection status), R1 (non in-sano resection), PSM (propensity score matching).







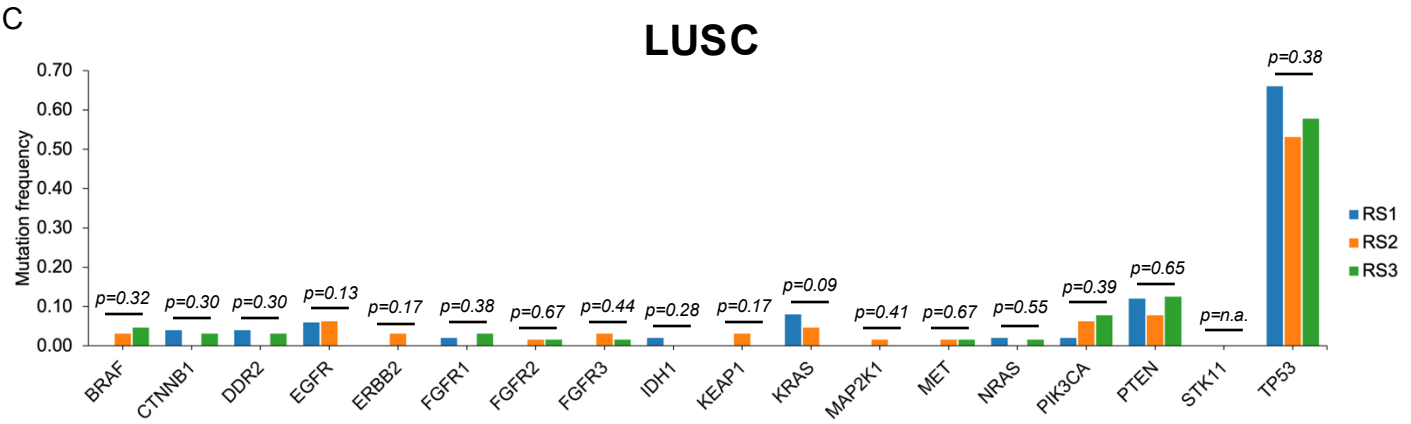
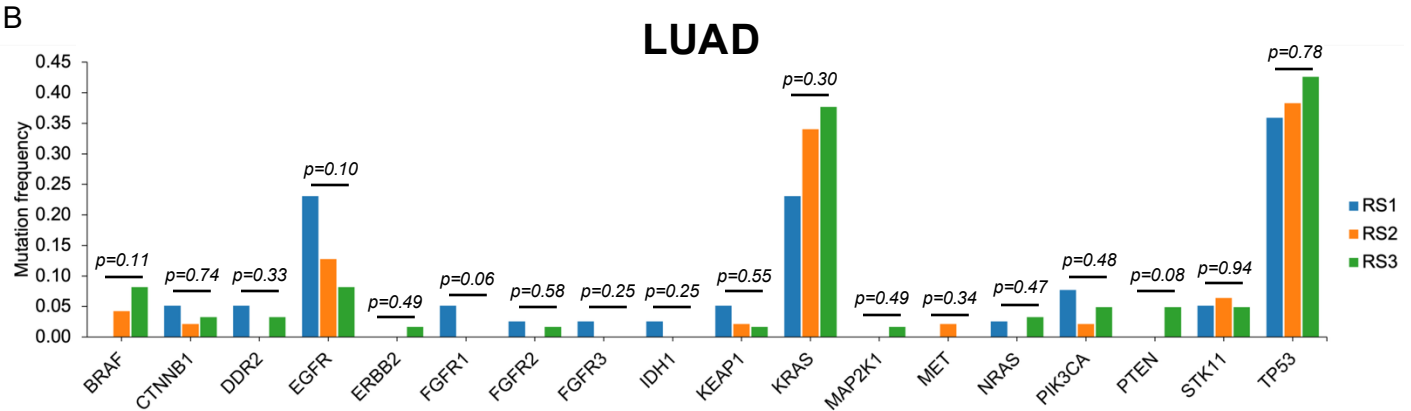
Supplementary Figure 14: Late-stage patients.
(A) LUAD late-stage patients UICC8=IV (n = 72).
(B) LUSC late-stage patients UICC8=IV (n = 18).
Separation tested significantly via log-rank test.



Supplementary Figure 15: Adjuvant patients.
(A) LUAD adjuvant patients (n = 164).
(B) LUSC adjuvant patients (n = 98).
Separation tested significantly via log-rank test.

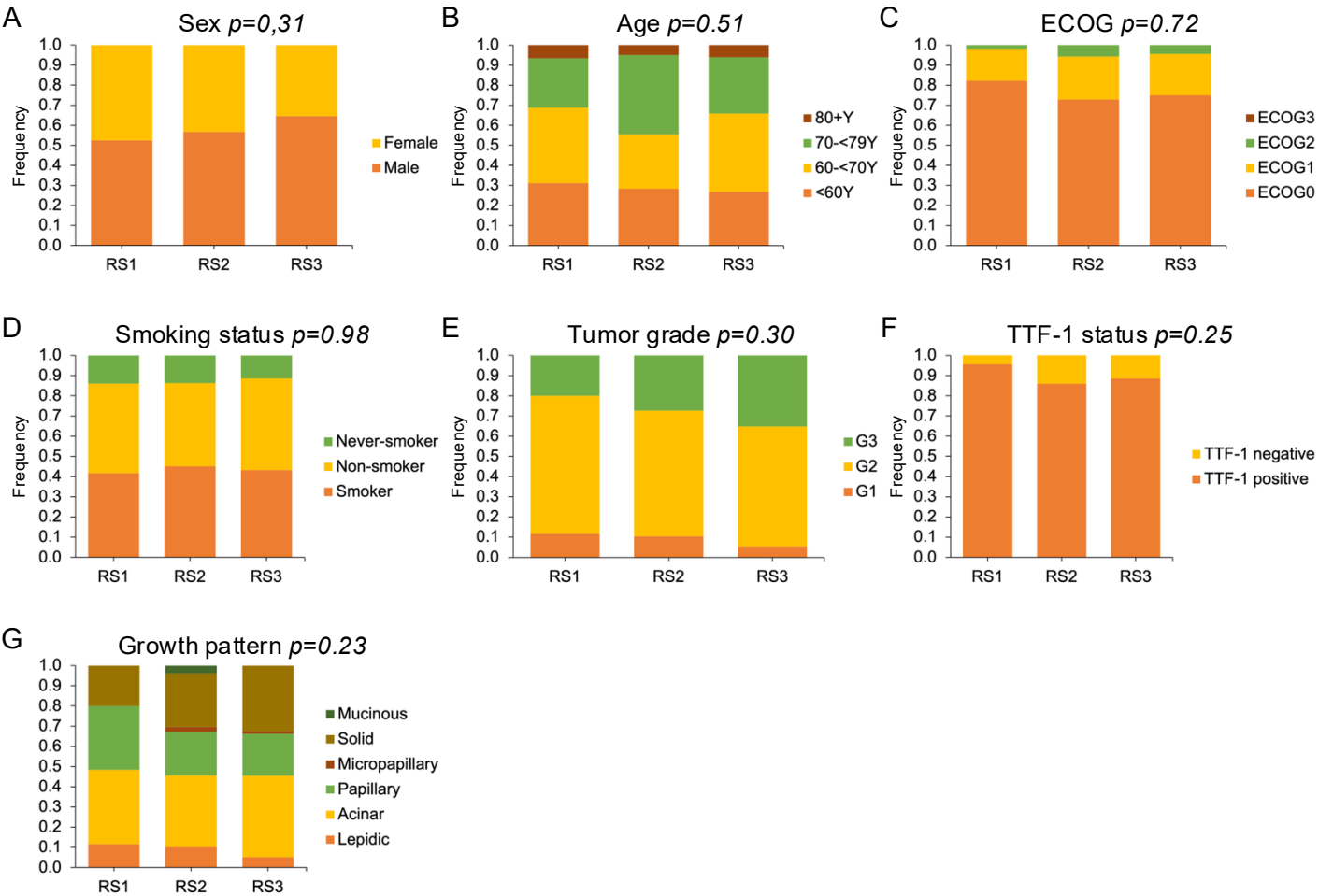
A

Gene	BRAF	CTNNB1	DDR2	EGFR	ERBB2	FGFR1	FGFR2	FGFR3	IDH1	KEAP1	KRAS	MAP2K1	MET	NRAS	PIK3CA	PTEN	STK11	TP53
Exon	11, 15	3	3-18	18-21	19,20	4-7, 10, 12-15	8-10, 12, 17, 20	7, 10, 15	4	2-6	2,3	2	14	2, 3	10, 21	1-8	2-7	5-8

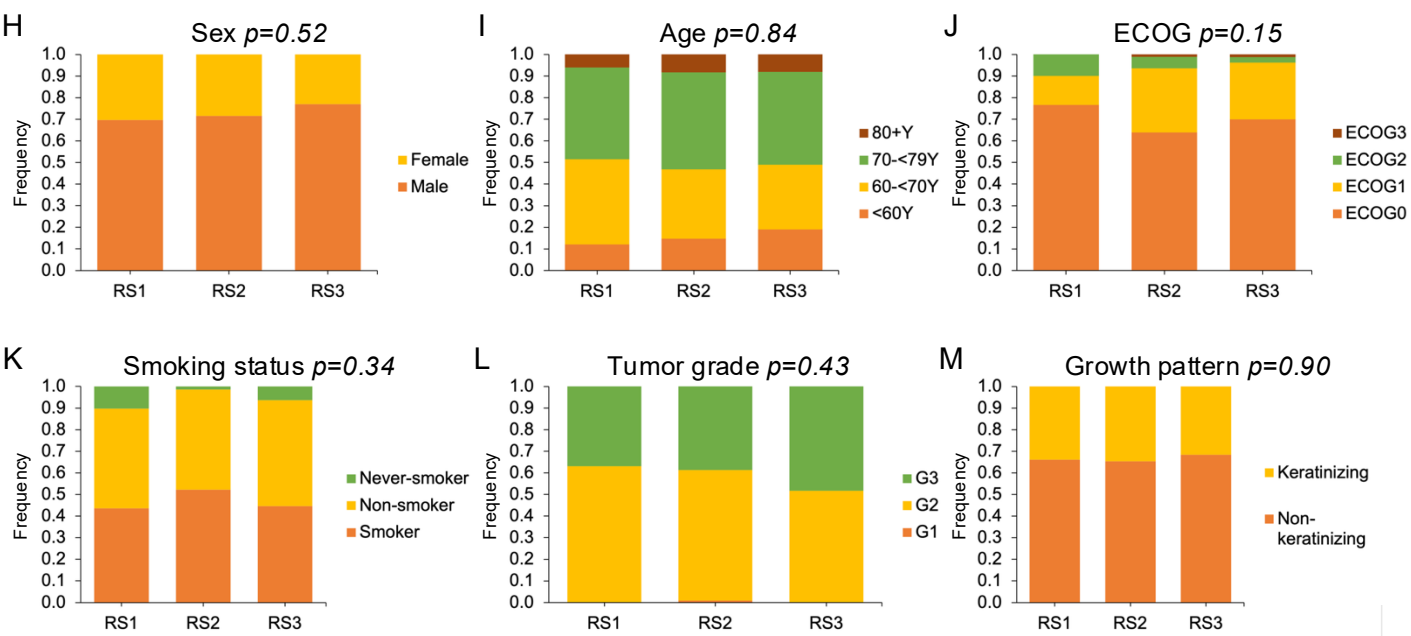


Supplementary Figure 16: Independence of cell-niche derived risk groups and mutation status.
 (A) Gene panel overview, including 18 essential genes for the molecular characterization of NSCLC.
 (B) Mutation frequencies across cell-niche-derived risk groups in LUAD tested for association using Chi-squared test (n = 147 patients).
 (C) Mutation frequencies across cell-niche-derived risk groups in LUSC tested for association using Chi-squared test (n = 178 patients).

LUAD



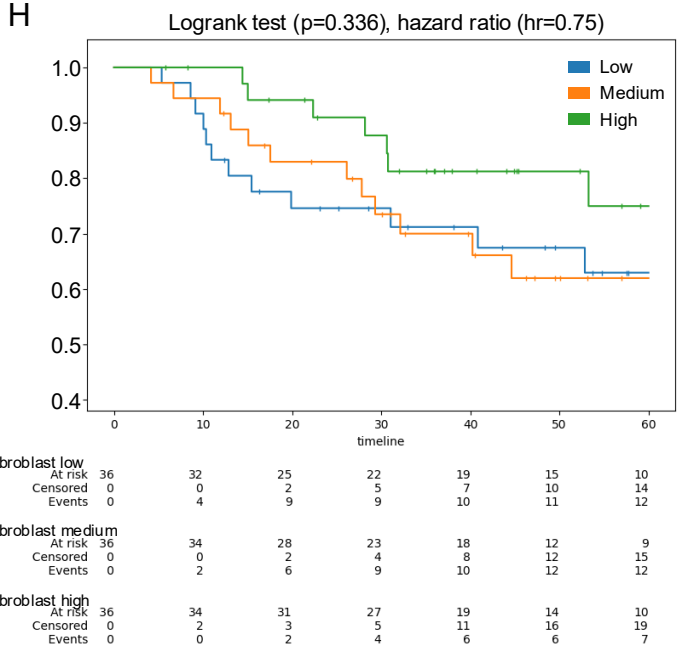
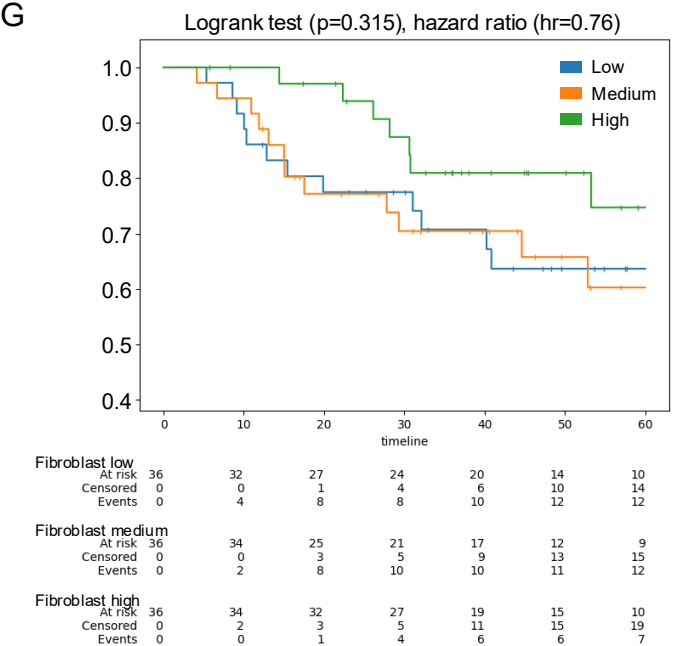
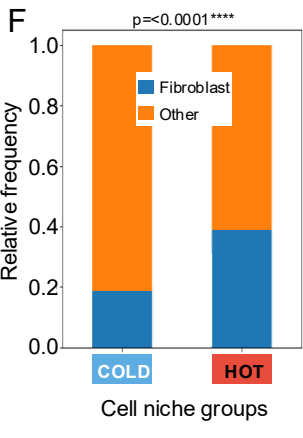
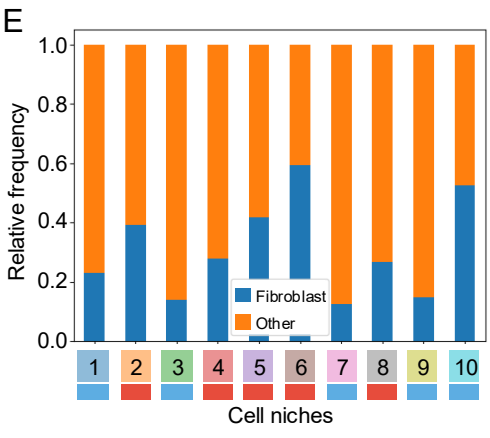
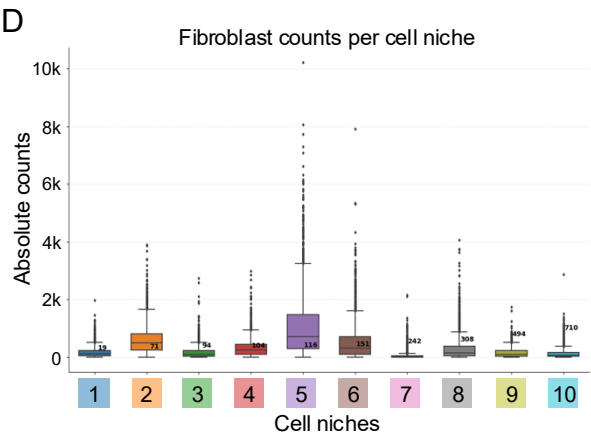
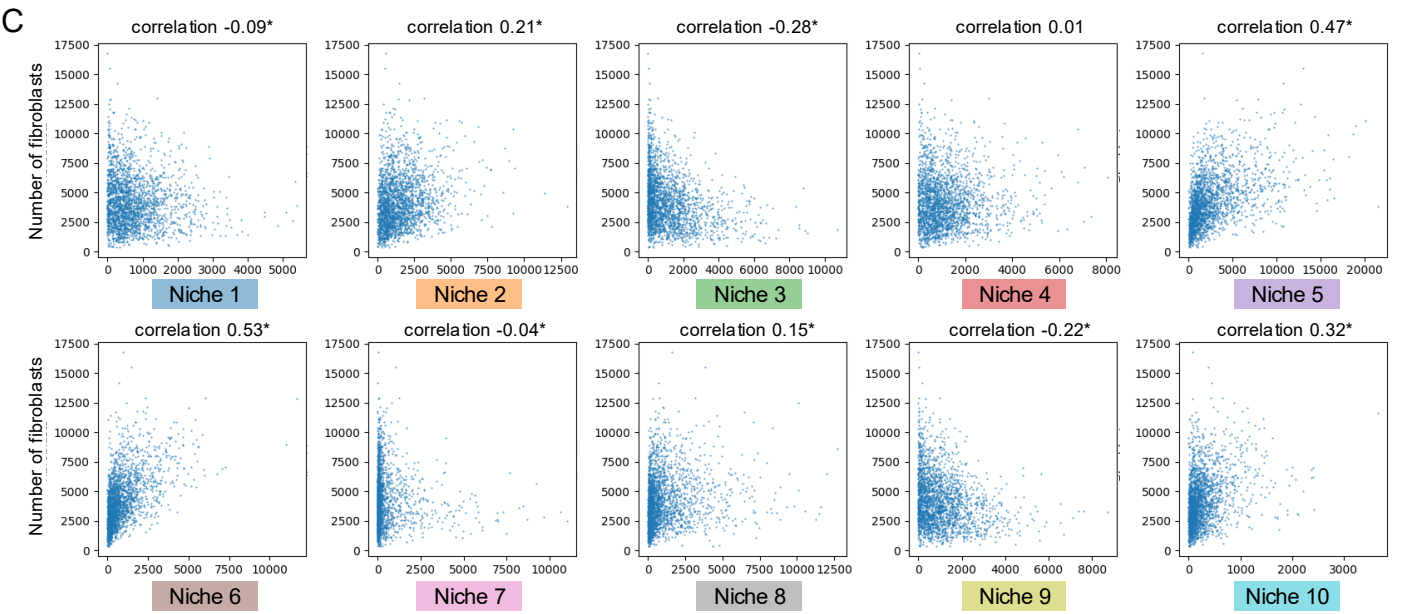
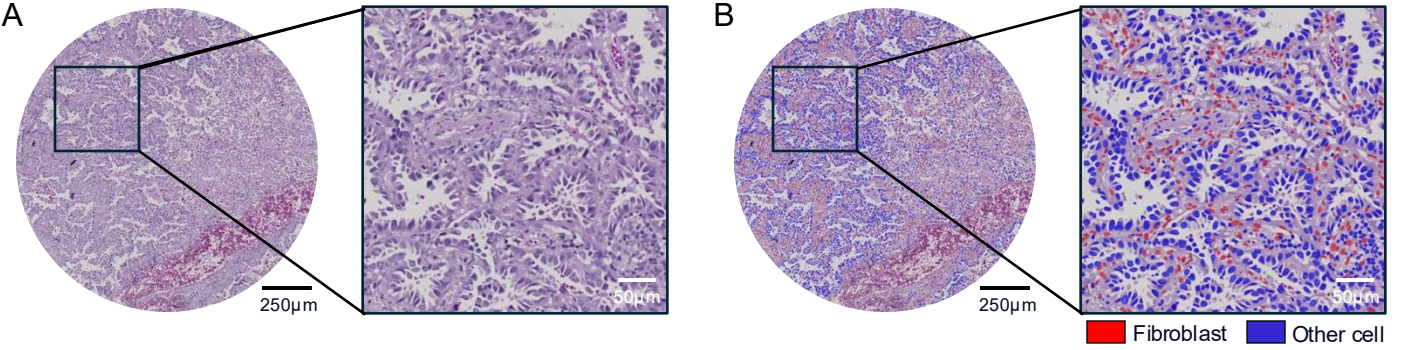
LUSC



Supplementary Figure 17: Cell-niche derived risk scores are independent of established clinicopathological covariates.

(A-G) Distribution of sex (n = 224 patients), age (n = 224 patients), ECOG performance status (n = 194 patients), smoking status (n = 131 patients), tumor grade (n = 211 patients), TTF-1 expression (n = 180 patients), and growth pattern (n = 216 patients) across cell-niche-derived risk groups in LUAD tested for association using Chi-squared test.

(H-M) Distribution of sex (n = 275 patients), age (n = 275 patients), ECOG performance status (n = 234 patients), smoking status (n = 156 patients), tumor grade (n = 256 patients), and growth pattern (n = 270 patients) across cell-niche-derived risk groups in LUSC tested for association using Chi-squared test.



Supplementary Figure 18: Fibroblast abundance across cell niches in LUAD.

(A) Representative H&E image of a tissue spot (n = 1) containing LUAD (left) and corresponding highmagnification zoom-in (right).

(B) Output of the cell classification model showing AI-derived fibroblast predictions (red polygons) and other cell predictions (blue polygons) for the same spot (n = 1) and corresponding zoomed region shown in (A).

(C) Correlation of fibroblast abundance with niche abundance across tissue spots (n = 2,189 from n = 663 patients); each dot represents one tissue spot. Statistical significance was assessed using Pearson's correlation (`scipy.stats.pearsonr`).

(D) Absolute fibroblast counts per cell niche (n = 663 patients).

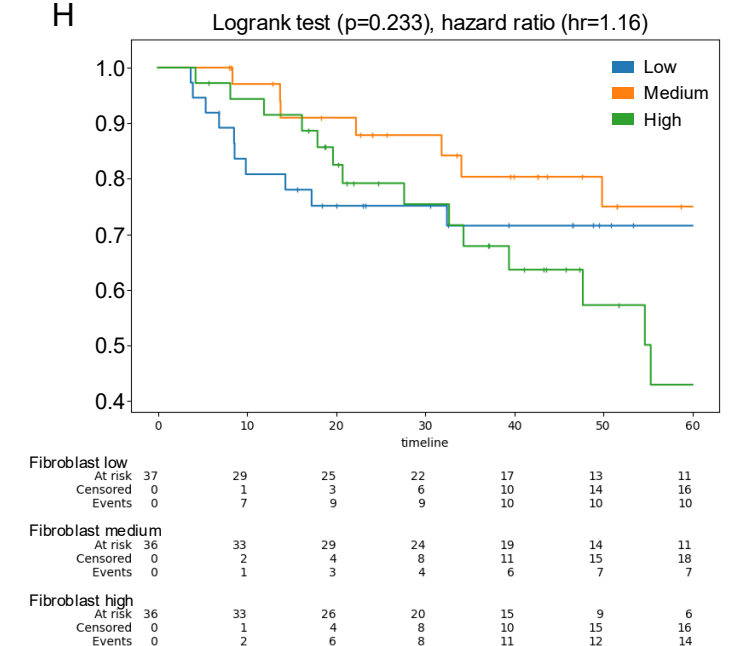
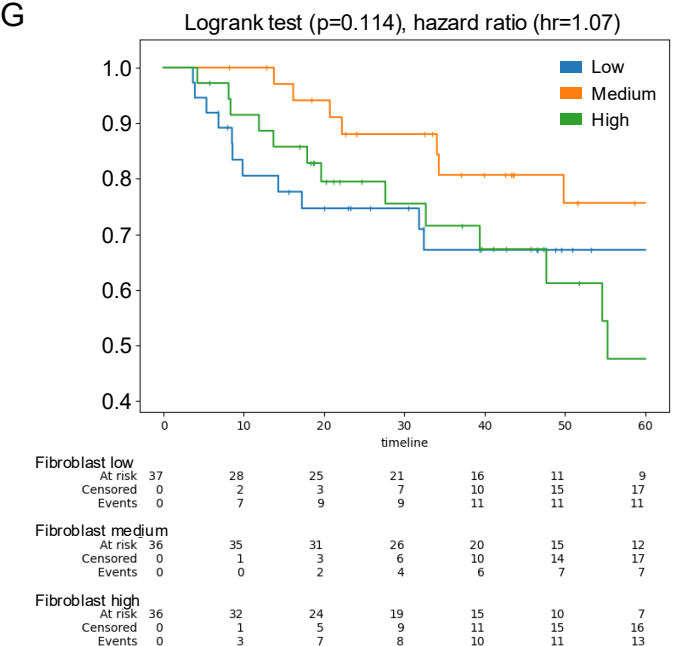
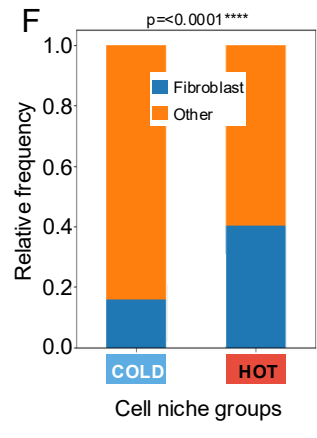
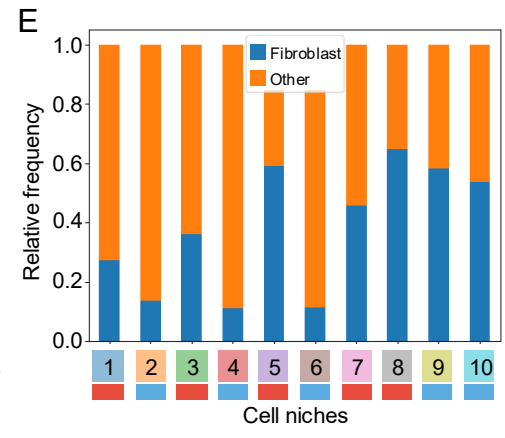
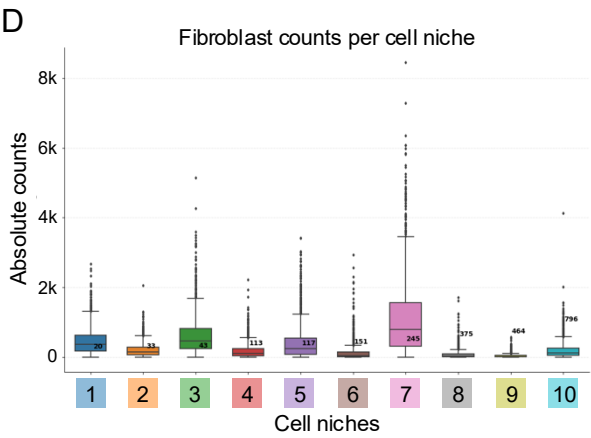
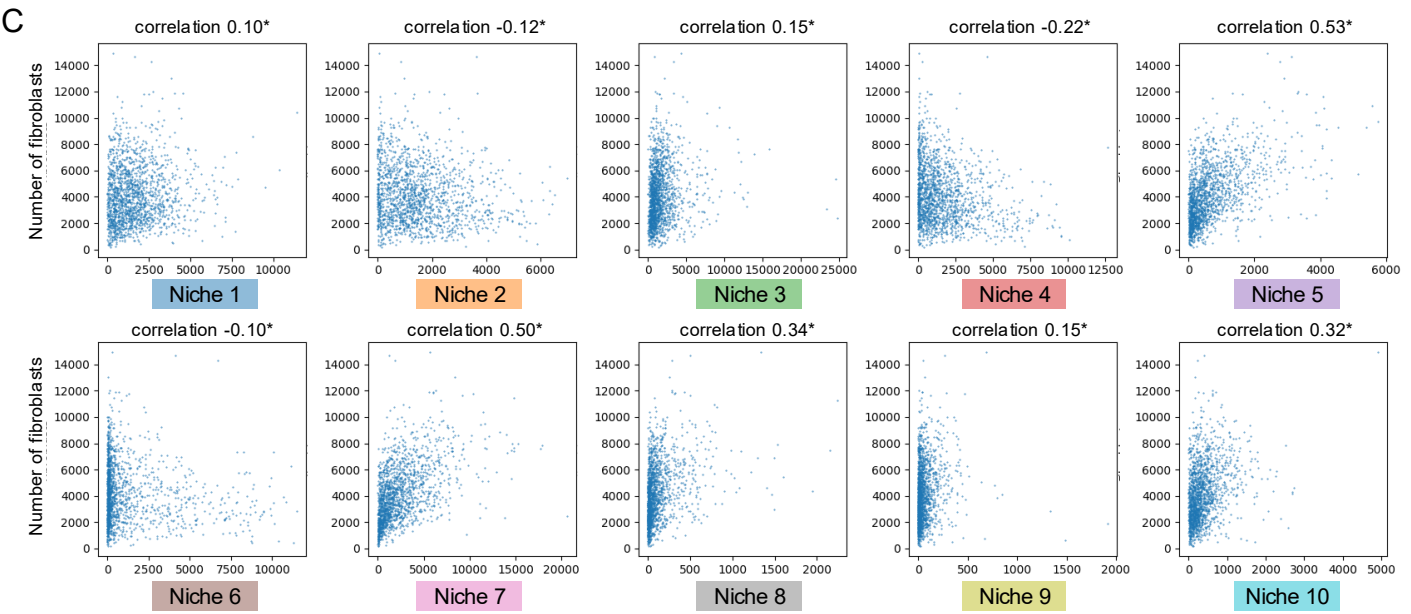
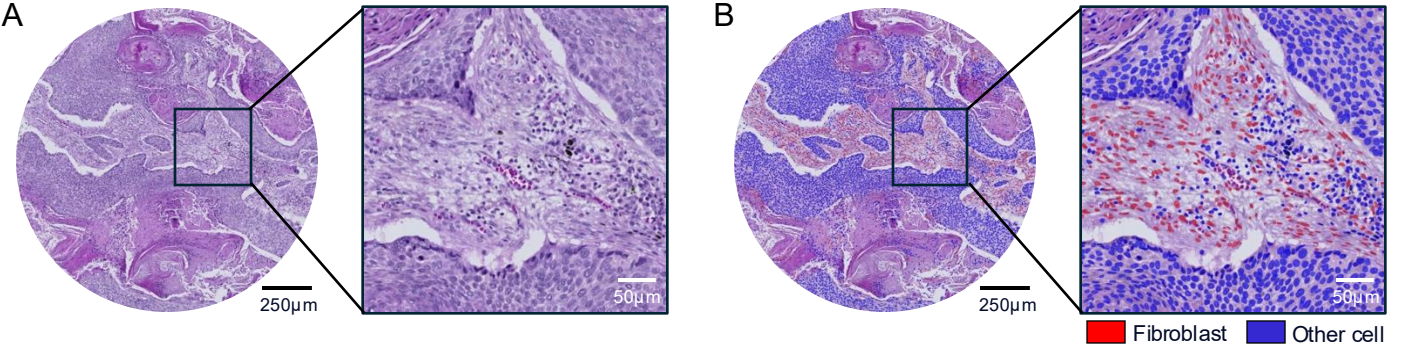
(E) Relative fibroblast frequency per cell niche, with niches classified as hot (red bar at bottom) or cold (blue bar at bottom; n = 663 patients).

(F) Relative fibroblast frequency within cold (left) and hot (right) niche groups (n = 663 patients). Statistical significance was assessed using a Chi-squared test.

(G) Kaplan-Meier analysis stratified by fibroblast maximum abundance over tissue spots per patient (max pooling); patients (n = 108) were divided into tertiles for direct comparison with cell niche pattern-based risk scores. Separation tested significantly via log-rank test.

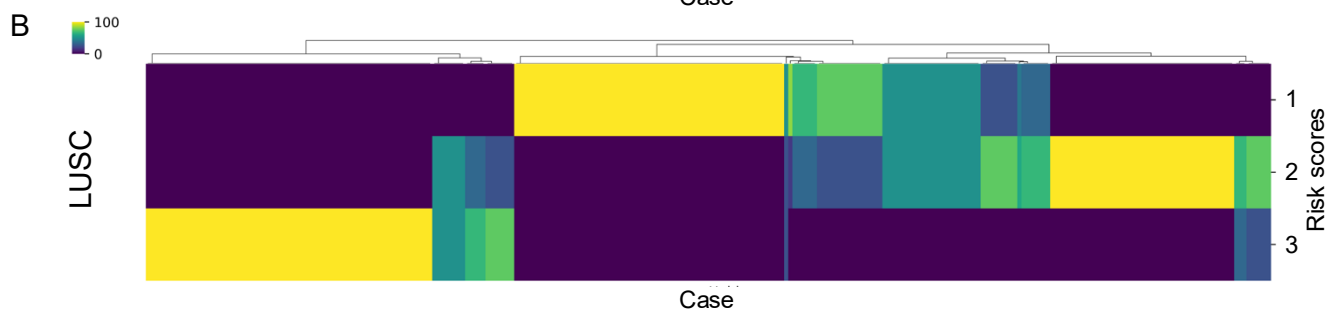
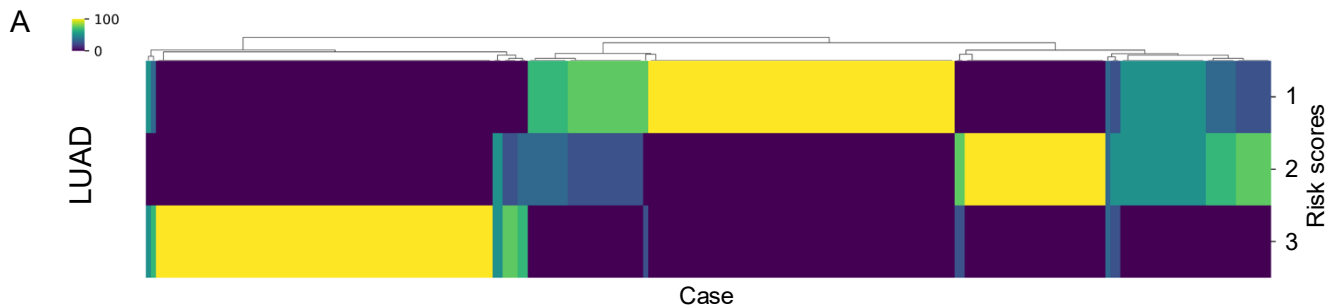
(H) Kaplan-Meier analysis stratified by fibroblast mean abundance over tissue spots per patient (n = 108); patients were divided into tertiles for direct comparison with cell niche pattern-based risk scores. Separation tested significantly via log-rank test.

Scale bars: (A+B) 250µm (tissue spots) and 50µm (magnified regions).



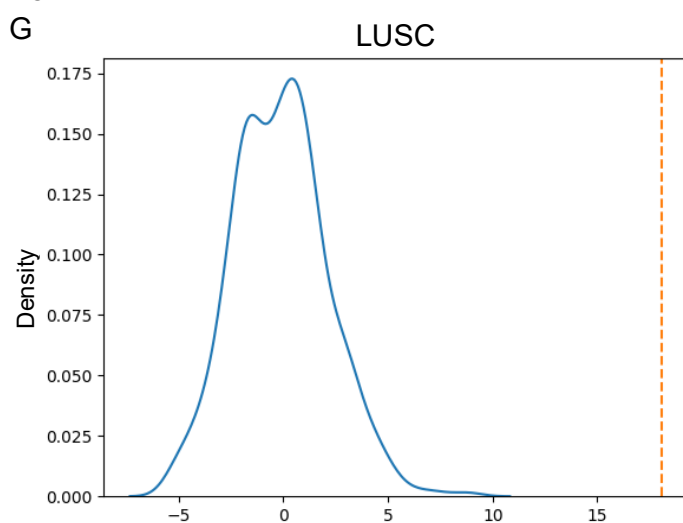
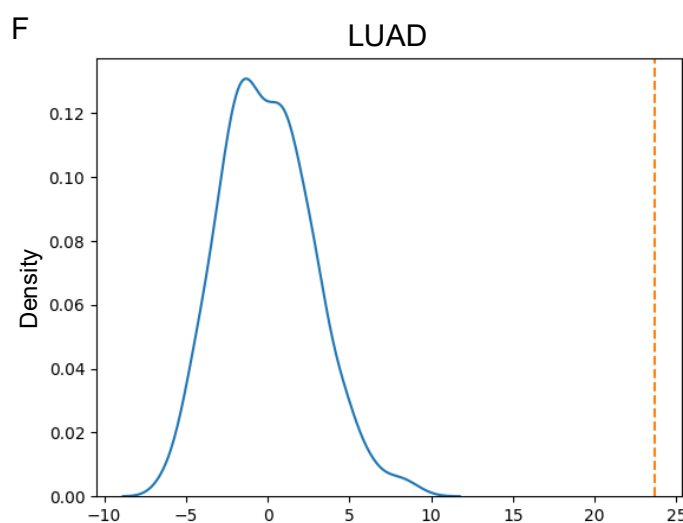
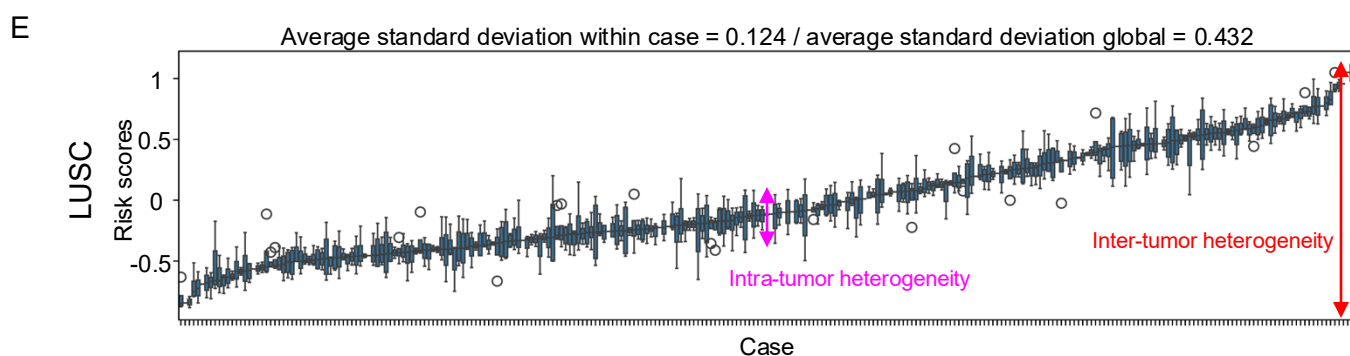
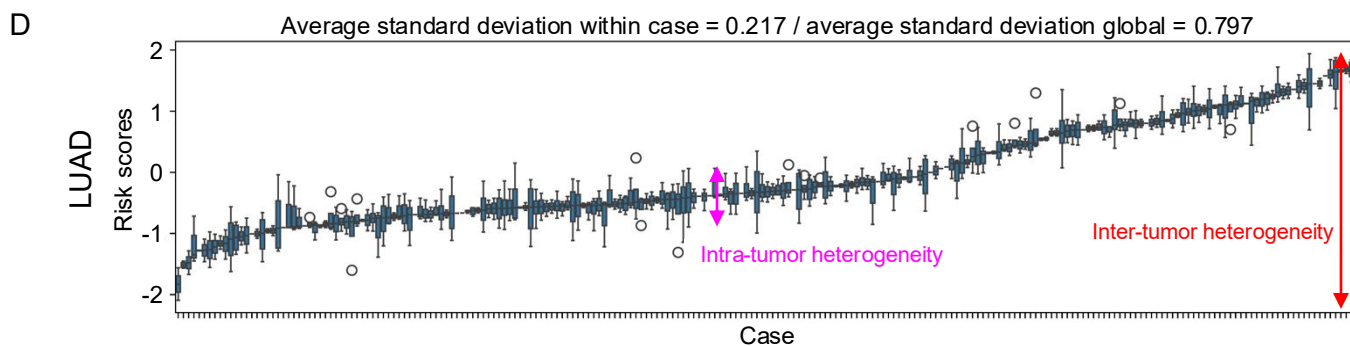
Supplementary Figure 19: Fibroblast abundance across cell niches in LUSC.

- (A) Representative H&E image of a tissue spot (n = 1) containing LUSC (left) and corresponding high magnification zoom-in (right).
- (B) Output of the cell classification model showing AI-derived fibroblast predictions (red polygons) and other cell predictions (blue polygons) for the same spot (n = 1) and corresponding zoomed region shown in (A).
- (C) Correlation of fibroblast abundance with niche abundance across tissue spots (n = 1,657 from n = 462 patients); each dot represents one tissue spot. Statistical significance was assessed using Pearson's correlation (`scipy.stats.pearsonr`).
- (D) Absolute fibroblast counts per cell niche (n = 462 patients).
- (E) Relative fibroblast frequency per cell niche, with niches classified as hot (red bar at bottom) or cold (blue bar at bottom; n = 462 patients).
- (F) Relative fibroblast frequency within cold (left) and hot (right) niche groups (n = 462 patients). Statistical significance was assessed using a Chi-squared test.
- (G) Kaplan-Meier analysis stratified by fibroblast maximum abundance over tissue spots per patient (max Pooling); patients (n = 108) were divided into tertiles for direct comparison with cell niche pattern-based risk scores. Separation tested significantly via log-rank test.
- (H) Kaplan-Meier analysis stratified by fibroblast mean abundance over tissue spots per patient (n = 109); patients were divided into tertiles for direct comparison with cell niche pattern-based risk scores. Separation tested significantly via log-rank test.
- Scale bars: (A+B) 250µm (tissue spots) and 50µm (magnified regions).



C

Core distribution by risk group	LUAD	LUSC
Patients with all 4 cores in the same risk group	70%	65%
Patients with $\geq 75\%$ of cores in the same risk group	75%	71%
Patients with $\geq 50\%$ of cores in the same risk group	87%	87%



Supplementary Figure 20: Comprehensive analysis of inter- and intra-tumor heterogeneity.

(A) LUAD: Cluster map illustrates the distribution of tissue spots ($n = 2,233$ from $n = 663$ patients), which have been assigned one of three risk scores. Yellow indicates cases where all tissue cores share the same risk score. Conversely, dark blue is used to indicate that no cores of one risk score are observed in a case. Green and blue represent cases with mixed scores. y-axis: risk score, x-axis: cases.

(B) Same as (A) but for LUSC ($n = 1,659$ tissue spots from $n = 462$ patients).

(C) Tissue core distribution by risk scores for LUAD ($n = 663$ patients) and LUSC ($n = 462$ patients). The results show a relatively high concordance/low heterogeneity with 70% (65%) of patients showing the same risk group in all 4 TMA cores.

(D) LUAD: Continuous risk score plot shows that intra-tumor heterogeneity is significantly lower than interpatient (inter-tumor) heterogeneity ($n = 663$ patients). y-axis: risk score, x-axis: cases. Each small box plot corresponds to one patient.

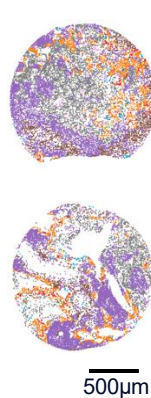
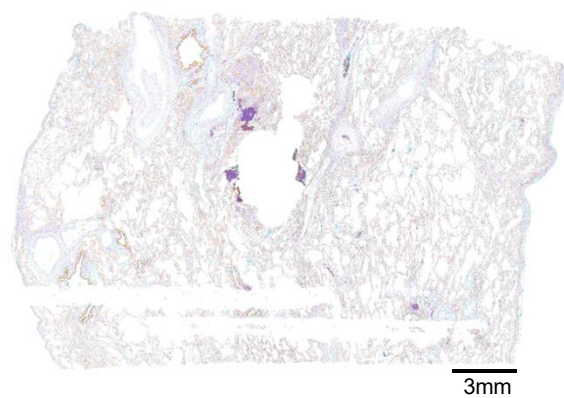
(E) Same as (D) but for LUSC ($n = 462$ patients).

(F+G) "Within-risk group" niche pattern variation is significantly lower than "between-risk group" variation in LUAD (F; $n = 663$ patients) and LUSC (G; $n = 462$ patients):

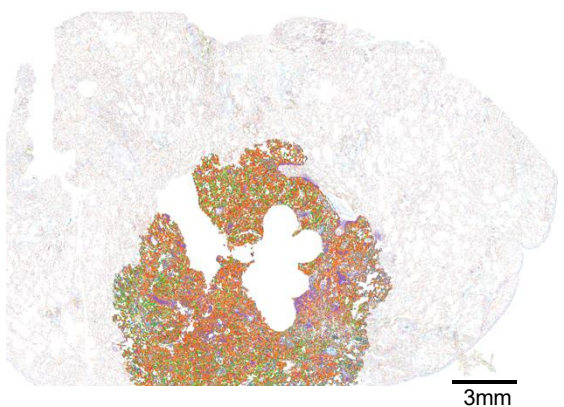
A permutation test was performed that compares the difference of niche pattern variation within the same risk group and the variation observed across the entire cohort ($p < 0.001^{****}$). Blue curve: distribution of results when the risk scores for the entire cohort were randomly shuffled (null hypothesis). Orange line: observed difference in variation (transport costs) using the actual risk groups.

Cell niches on whole tumor sections and tissue cores

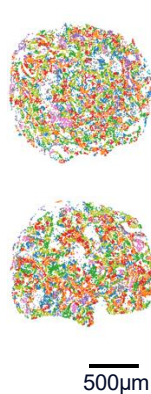
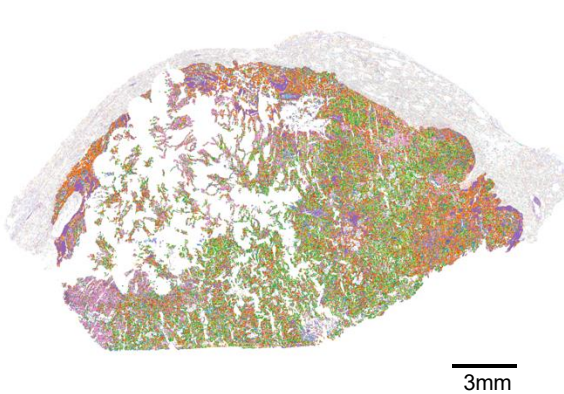
LUAD RISK SCORE 1



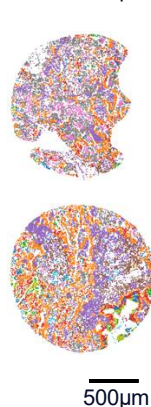
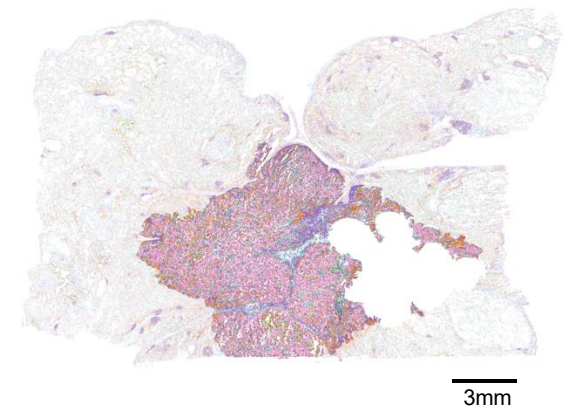
LUAD RISK SCORE 1



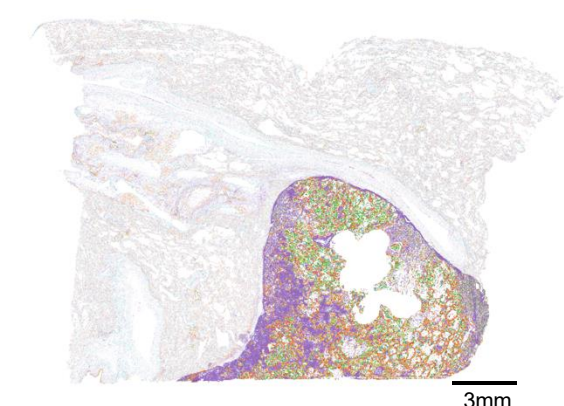
LUAD RISK SCORE 2



LUAD RISK SCORE 2



LUAD RISK SCORE 2

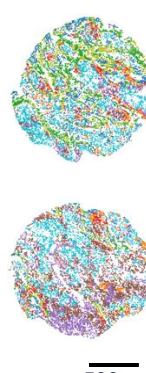
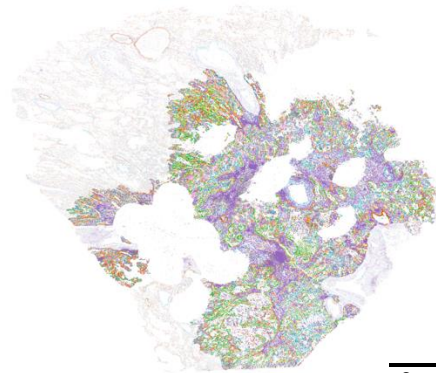
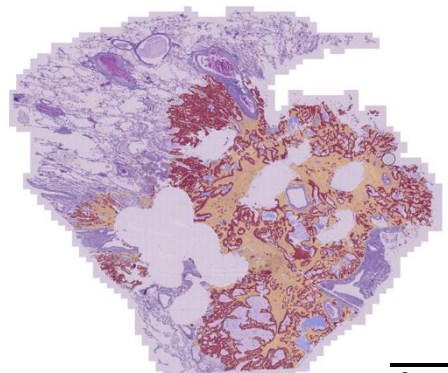


F

Tissue segmentation

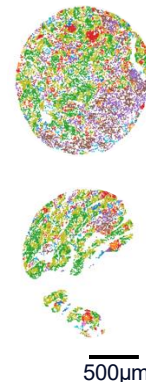
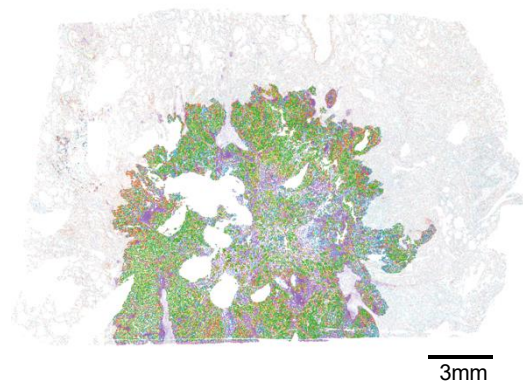
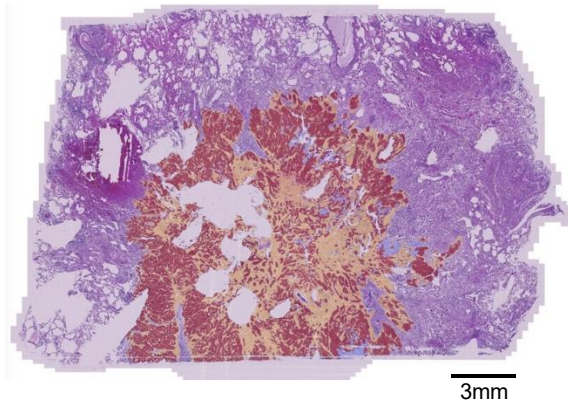
Cell niches on whole tumor sections and tissue cores

LUAD RISK SCORE 1



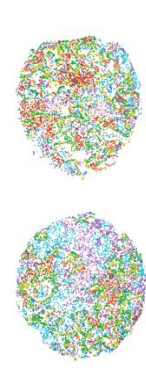
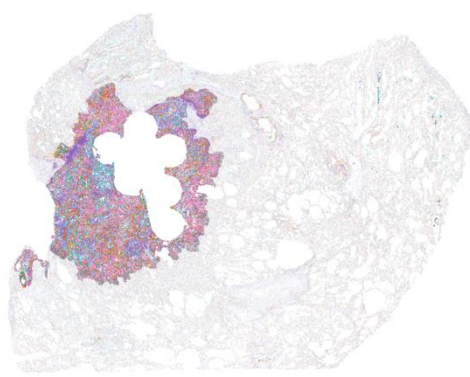
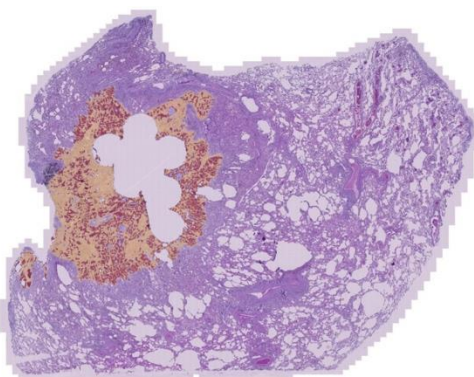
G

LUAD RISK SCORE 1



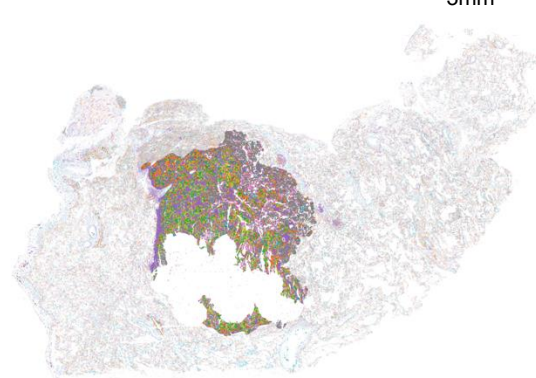
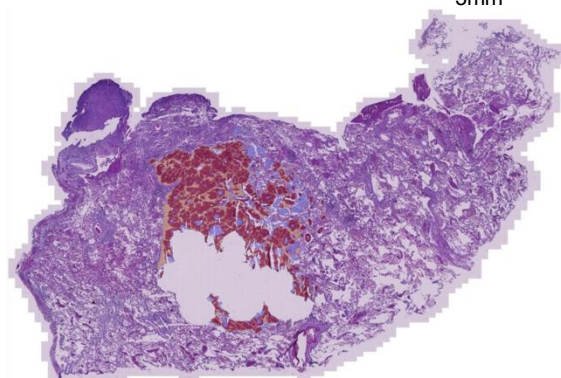
H

LUAD RISK SCORE 2



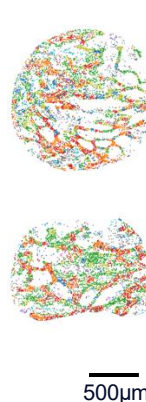
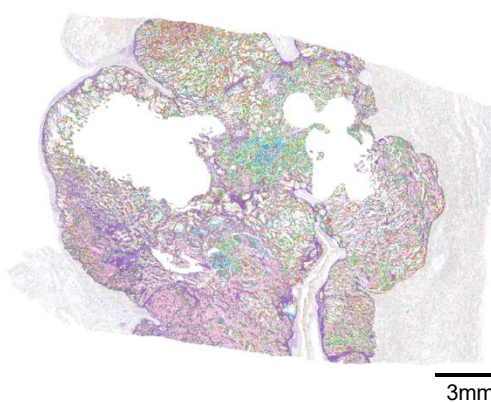
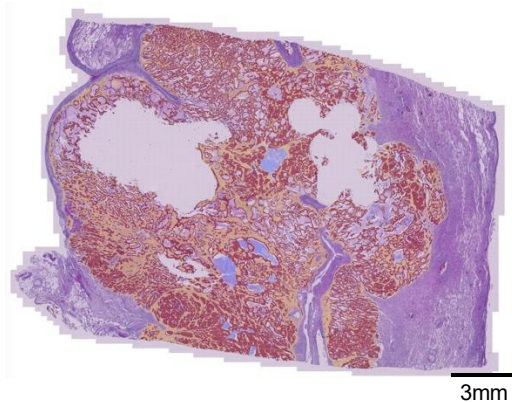
1

LUAD RISK SCORE 2



J

LUAD RISK SCORE 2



Supplementary Figure 21: Niche pattern on whole tumor sections and corresponding tissue cores in LUAD.

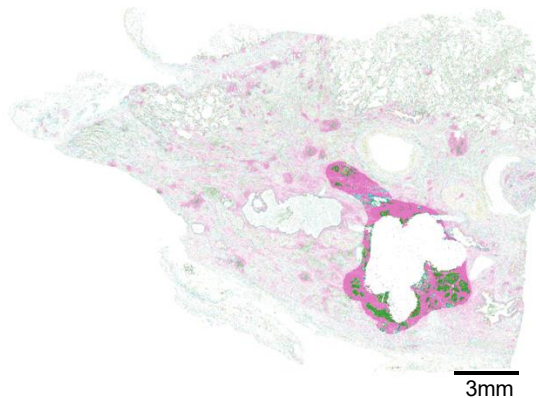
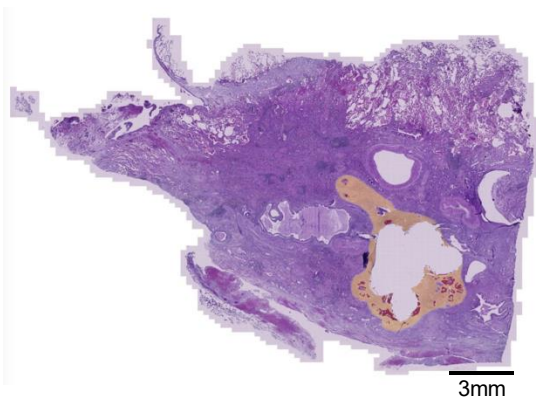
(A+B) H&E-stained whole tumor section (n = 2 tumor samples) with AI-derived tissue segmentation (left; carcinoma = red, stroma = yellow, necrosis = blue, healthy tissue = uncolored), same whole tumor section with niche patterns of risk score 1 (center) and two corresponding tissue cores with niche patterns of risk score 1 (right).
(C-F) Same as (A) but for risk score 2 (n = 4 tumor samples).
(G-J) Same as (A) but for risk score 3 (n = 4 tumor samples).
Scale bars: (A-J) 3mm (whole tumor sections) and 500µm (tissue spots)

A

Tissue segmentation

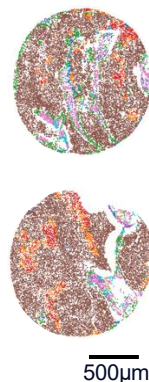
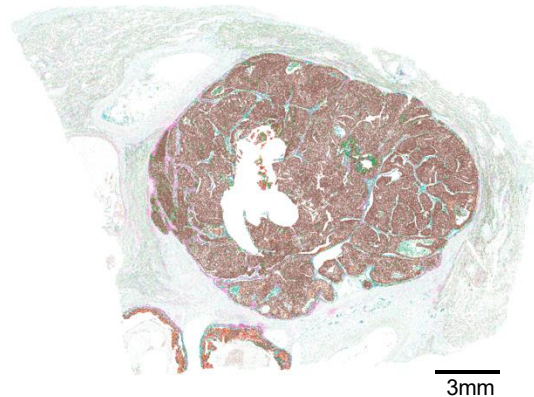
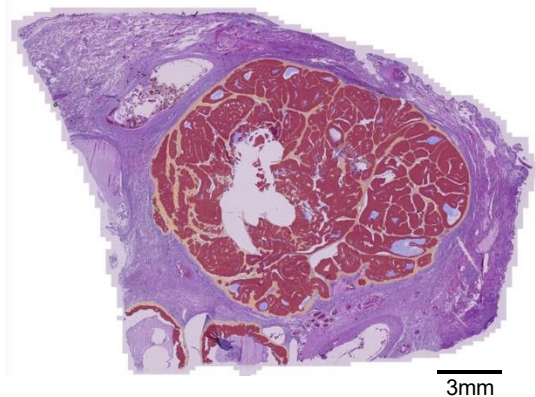
Cell niches on whole tumor sections and tissue cores

LUAD RISK SCORE 1



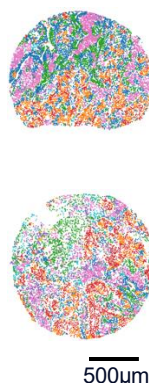
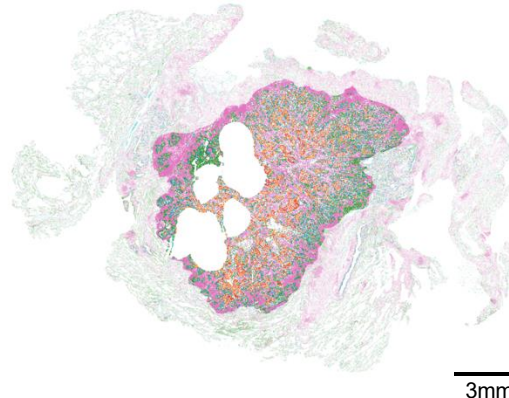
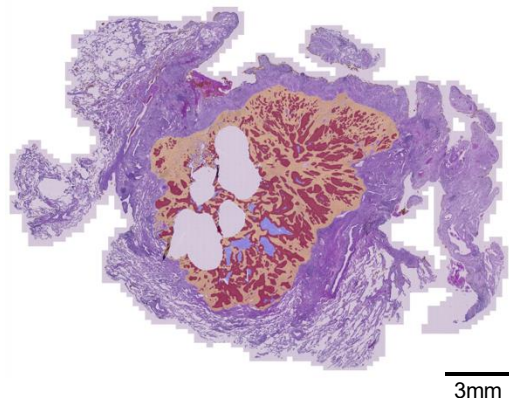
B

LUAD RISK SCORE 1



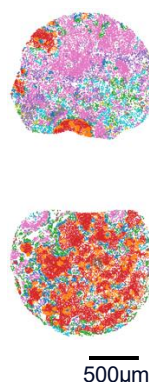
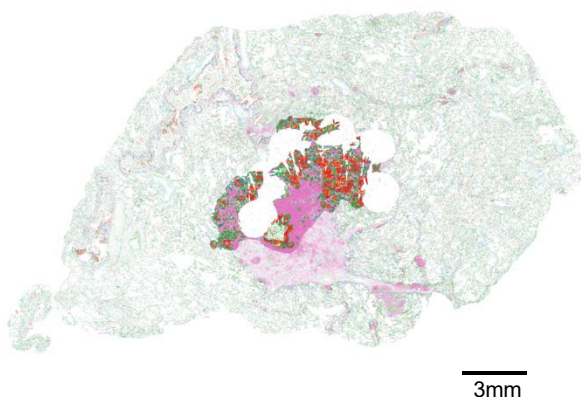
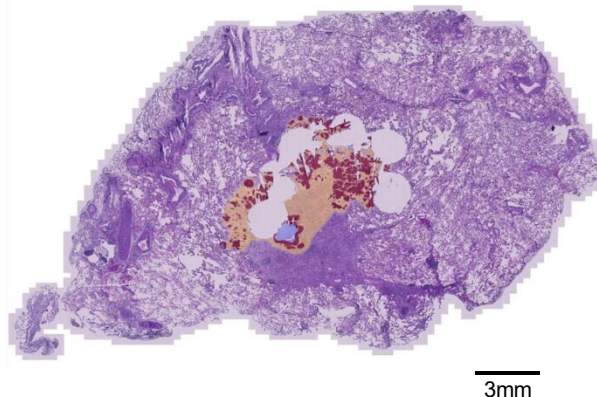
C

LUNG RISK SCORE 2



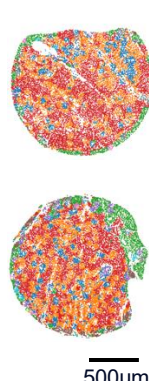
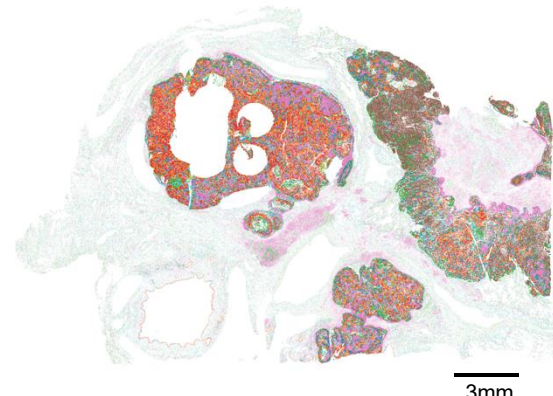
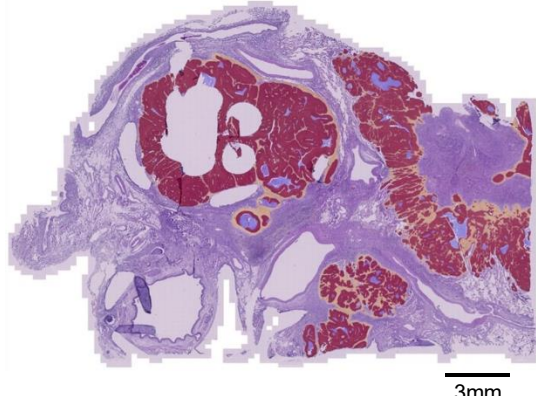
D

LUAD RISK SCORE 2



E

- UAD RISK SCORE 2

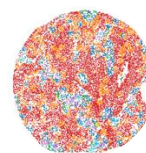
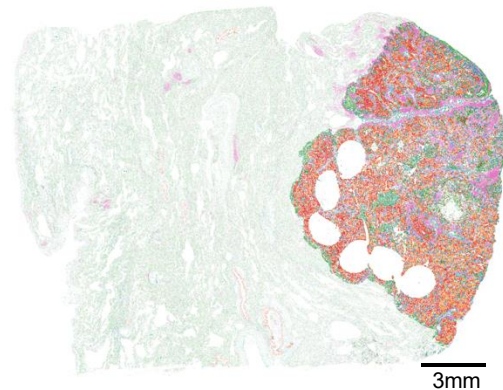
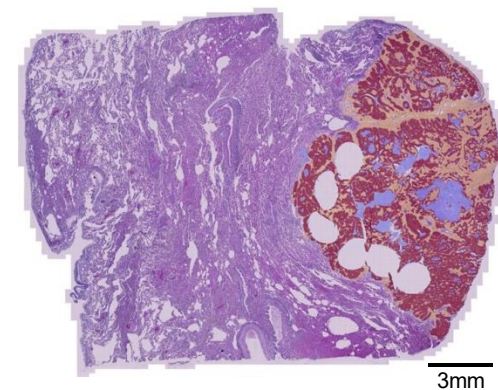


F

Tissue segmentation

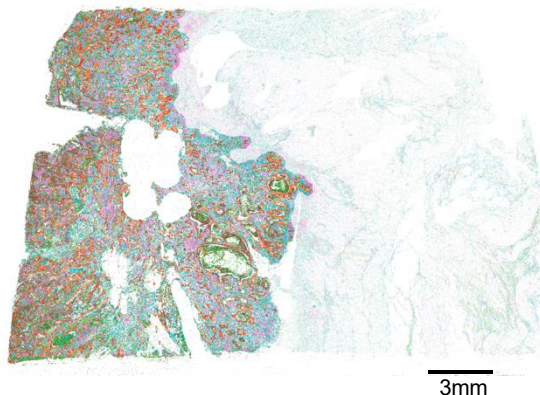
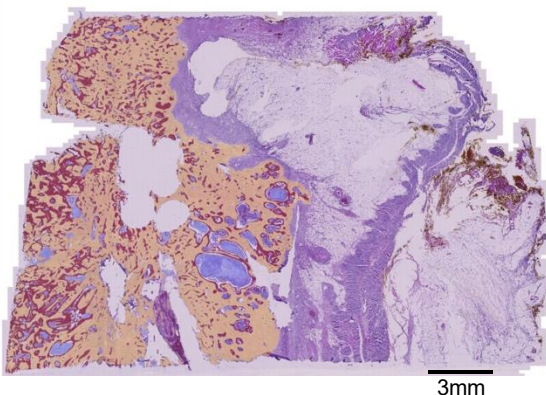
Cell niches on whole tumor sections and tissue cores

LUAD RISK SCORE 1



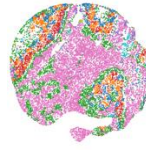
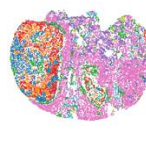
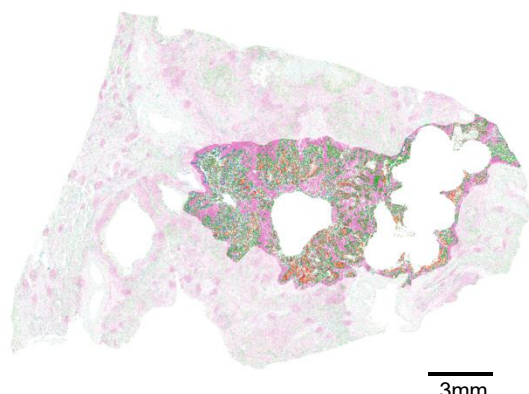
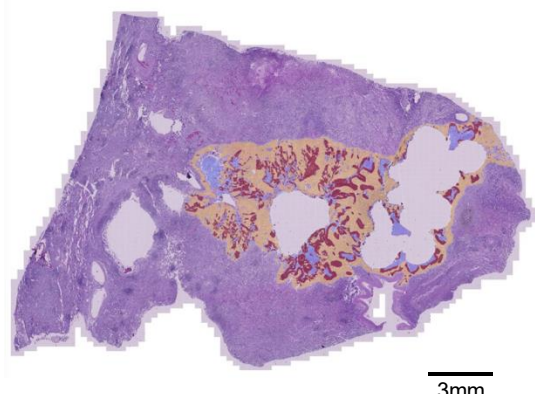
G

LUAD RISK SCORE 1



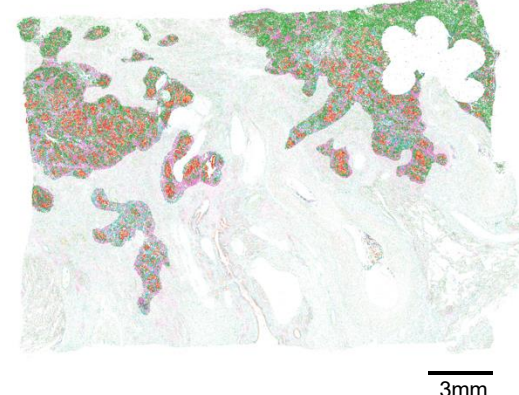
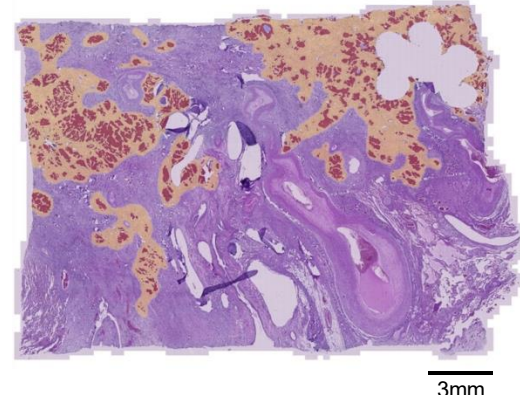
H

LUAD RISK SCORE 2



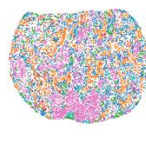
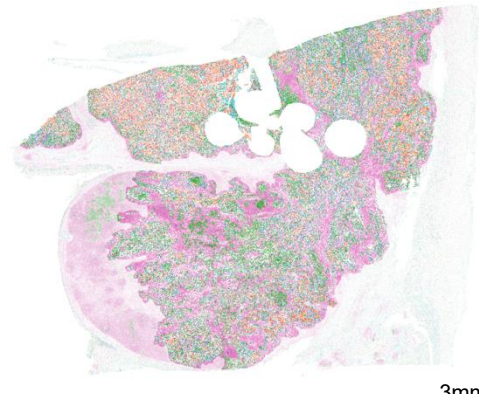
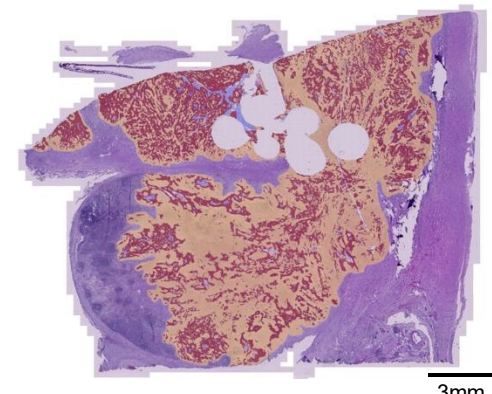
1

LUAD RISK SCORE 2



J

LUAD RISK SCORE 2



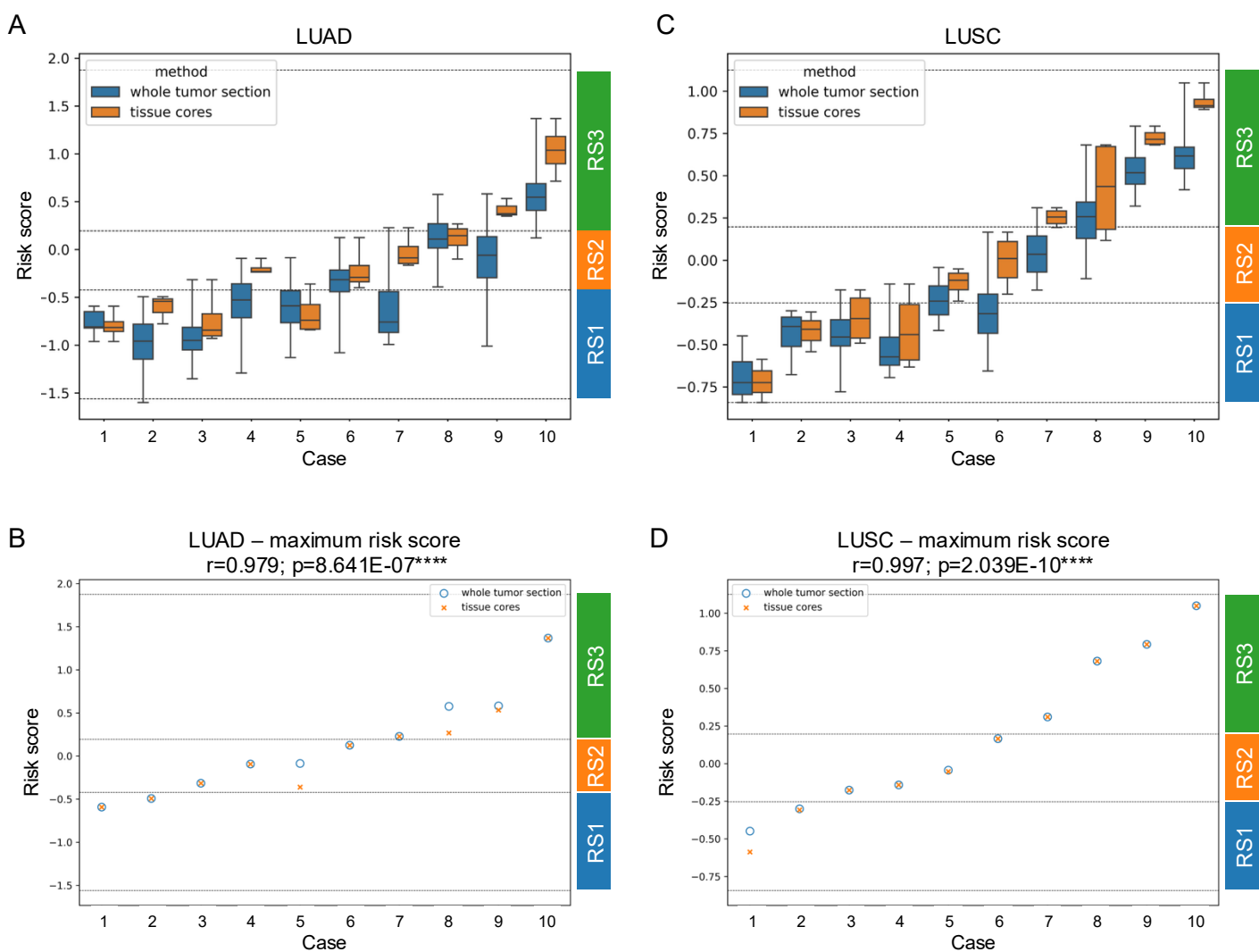
Supplementary Figure 22: Niche pattern on whole tumor sections and corresponding tissue cores in LUSC.

(A+B) H&E-stained whole tumor section (n = 2 tumor samples) with AI-derived tissue segmentation (left; carcinoma = red, stroma = yellow, necrosis = blue, healthy tissue = uncolored), same whole tumor section with niche patterns of risk score 1 (center) and two corresponding tissue cores with niche patterns of risk score 1 (right).

(C-F) Same as (A) but for risk score 2 (n = 4 tumor samples).

(G-J) Same as (A) but for risk score 3 (n = 4 tumor samples).

Scale bars: (A-J) 3mm (whole tumor sections) and 500µm (tissue spots)



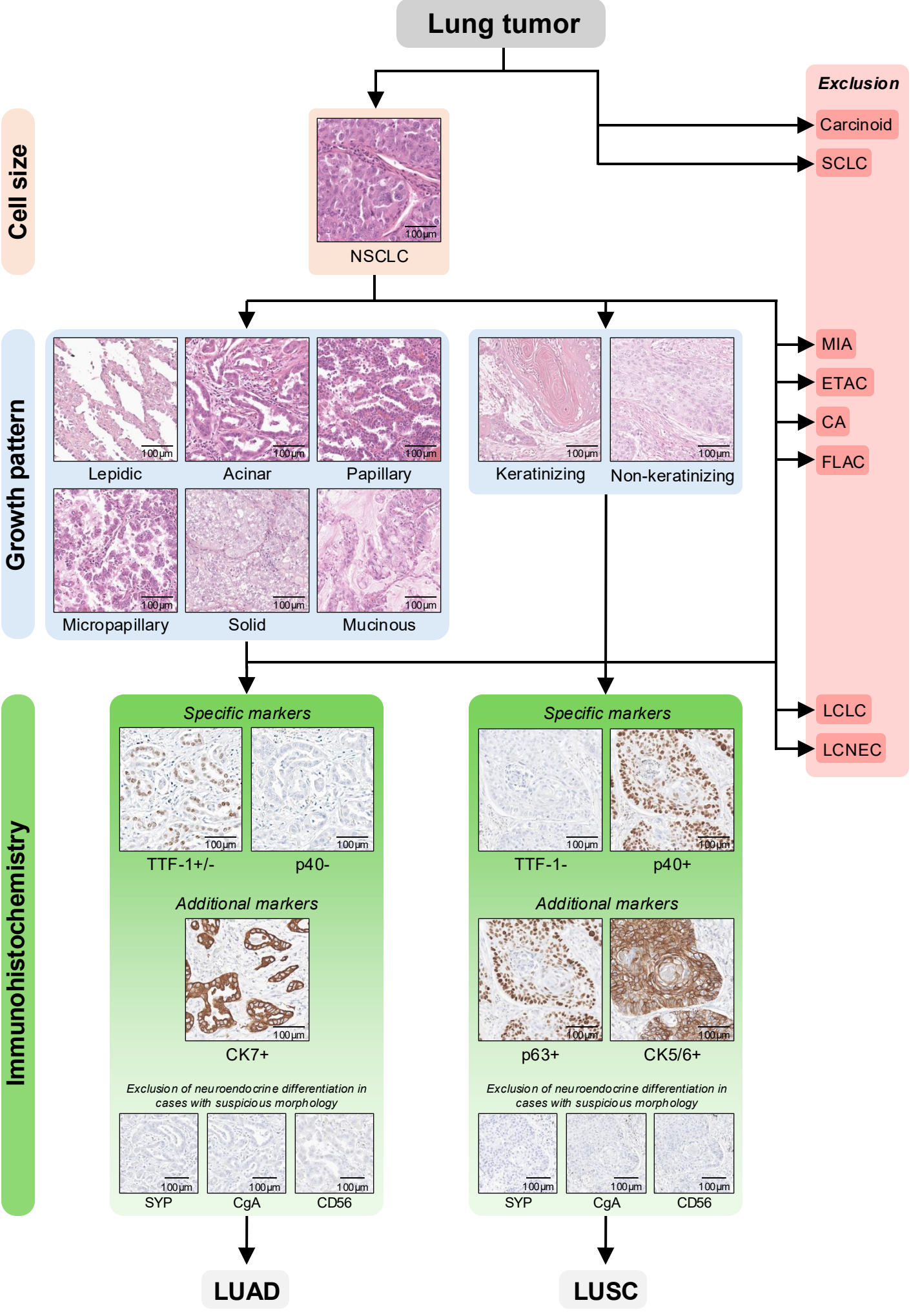
Supplementary Figure 23: Concordance of risk scores between whole tumor sections and corresponding tissue cores.

(A) LUAD risk score distribution ($n = 10$ patients): A continuous risk score plot shows risk score distributions within the whole tumor sections (blue) and corresponding tissue microarray cores (orange). y-axis: risk score, x-axis: cases (ordered by increasing mean risk), horizontal lines show boundaries between risk scores. Box plots show the median (center line), interquartile range Q1–Q3 (box), and whiskers to the most extreme points within $1.5 \times \text{IQR}$.

(B) LUAD risk score concordance ($n = 10$ patients): Risk scores (maximum risk) for whole tumor sections (blue circles) are highly correlated with tissue core risk scores (orange crosses). Risk group assignments (RS1–3) are 100% concordant. y-axis: risk score, x-axis: cases (ordered by increasing final risk score), horizontal lines show boundaries between risk scores. Box plots show the median (center line), interquartile range Q1–Q3 (box), and whiskers to the most extreme points within $1.5 \times \text{IQR}$.

(C) LUSC risk score distribution ($n = 10$ patients): Same as (A) but for LUSC. Statistical significance was assessed using Pearson's correlation (`scipy.stats.pearsonr`).

(D) LUSC risk score concordance ($n = 10$ patients): Same as (B) but for LUSC. Statistical significance was assessed using Pearson's correlation (`scipy.stats.pearsonr`).



Supplementary Figure 24: Diagnostic workflow and case selection criteria for lung cancer specimens.

Schematic overview of the diagnostic work-up based on histomorphology and immunohistochemistry, including inclusion and exclusion criteria applied for LUAD and LUSC case selection (n = 11 representative tumor samples). Rare tumor types and neuroendocrine neoplasms were excluded as outlined.

NSCLC, non-small cell lung cancer; SCLC, small-cell lung carcinoma; MIA, minimally invasive adenocarcinoma; ETAC, enteric-type adenocarcinoma; CA, colloid adenocarcinoma; FLAC, fetal adenocarcinoma; LCLC, large-cell lung carcinoma; LCNEC, large-cell neuroendocrine carcinoma; TTF-1, thyroid transcription factor 1; CK, cytokeratin; SYP, Synaptophysin; CgA, Chromogranin A; LUAD, lung adenocarcinoma; LUSC, lung squamous cell carcinoma.

Scale bars: 100µm

	Standard stardist		Standard stardist (DAPI)		In-house (H&E)	
Case number	recall (sensitivity)	precision (PPV)	recall (sensitivity)	precision (PPV)	recall (sensitivity)	precision (PPV)
1	0.496	0.990	0.962	0.830	0.959	0.872
2	0.417	0.981	0.886	0.849	0.941	0.902
3	0.639	0.996	0.923	0.858	0.934	0.919
4	0.509	0.975	0.848	0.800	0.880	0.941
5	0.260	0.990	0.811	0.868	0.904	0.942
6	0.276	0.644	0.916	0.788	0.823	0.933
7	0.667	0.993	0.933	0.838	0.952	0.881
8	0.670	0.974	0.875	0.912	0.923	0.953
9	0.383	0.982	0.952	0.719	0.962	0.921
10	0.537	1.000	0.897	0.846	0.937	0.959
11	0.517	0.896	0.902	0.770	0.919	0.881
12	0.798	0.829	0.920	0.858	0.901	0.908
13	0.594	0.940	0.802	0.867	0.948	0.834
14	0.822	0.899	0.922	0.851	0.897	0.970
15	0.653	0.982	0.955	0.802	0.961	0.955
16	0.394	0.993	0.806	0.848	0.872	0.941
17	0.539	0.978	0.913	0.785	0.827	0.934
18	0.441	0.888	0.810	0.744	0.792	0.867
19	0.496	0.986	0.908	0.826	0.911	0.945
20	0.578	0.952	0.910	0.831	0.902	0.949
21	0.311	0.974	0.836	0.751	0.845	0.953
22	0.193	0.980	0.926	0.765	0.897	0.874
23	0.727	0.959	0.917	0.867	0.919	0.954
24	0.734	0.969	0.789	0.907	0.902	0.946
25	0.436	1.000	0.923	0.842	0.873	0.950
global	0.531	0.952	0.884	0.825	0.903	0.924
F1-score	0.682		0.855		0.913	

Supplementary Table 1: Comparative performance analysis of cell detection models

	Specific immune states										
Subtype	PD-L1+/TIL+		PD-L1+/TIL-		PD-L1-/TIL+		PD-L1-/TIL-		PD-L1+/-/TIL-B+		P-value
LUAD	218	0.16	186	0.14	392	0.30	124	0.09	405	0.31	1.517E-62****
LUSC	340	0.28	259	0.21	300	0.24	245	0.20	86	0.07	

	Specific immune states				
Subtype	PD-L1+/TIL+		Other		P-value
LUAD	224	0.10	2009	0.90	4.724E-20****
LUSC	340	0.20	1319	0.80	

	Specific immune states				
Subtype	PD-L1+/TIL-		Other		P-value
LUAD	191	0.09	2042	0.91	9.765E-12****
LUSC	259	0.16	1400	0.84	

	Specific immune states				
Subtype	PD-L1-/TIL+		Other		P-value
LUAD	392	0.18	1841	0.82	0.67
LUSC	300	0.18	1359	0.82	

	Specific immune states				
Subtype	PD-L1-/TIL-		Other		P-value
LUAD	124	0.06	2109	0.94	2.885E-22****
LUSC	245	0.15	1414	0.85	

	Specific immune states				
Subtype	PD-L1+/-/TIL-B+		Other		P-value
LUAD	719	0.32	1514	0.68	4.367E-94****
LUSC	86	0.05	1573	0.95	

Supplementary Table 2: Comparative analysis of immune cell and niche composition in LUAD and LUSC

Statistical analysis was performed using two-sided Chi-Square tests.

Abbreviations: LUAD, lung adenocarcinoma; LUSC, lung squamous cell carcinoma; PD-L1, programmed death-ligand 1; TIL, tumor-infiltrating lymphocyte; TIL-B, tumor-infiltrating B cell.

* = p < 0.05; ** = p < 0.01; *** = p < 0.001; **** = p < 0.0001.

	LUAD	LUSC
UICC8 (state of the art)	0.633 [0.541 - 0.723]	0.637 [0.540 - 0.729]
Cellomics Density	0.644 [0.546 - 0.738]	0.674 [0.565 - 0.773]
Cellomics Niches	0.665 [0.566 - 0.758]	0.692 [0.597 - 0.781]

Supplementary Table 3: Survival prediction results in c-scores

	1	2	3	4	5	6	7	8	9	10
Activated B cell	1.041	2.373	0	1.462	3.426	1.204	0.903	1.892	0.699	0.301
Activated cytotoxic T cell	2.34	4.25	0	3.817	4.403	2.407	2.365	4.033	1.949	1.079
Activated natural killer cell	2.161	2.711	0	2.441	2.999	1.342	1.519	2.375	2.199	1
B cell	3.344	4.587	1.079	3.632	5.496	4.129	2.665	3.943	3.418	2.766
CD8+ T cell	3.117	4.717	0	4.152	5.238	4.027	2.813	4.335	3.305	2.294
Carcinoma cell	5.91	5.923	6.246	6.096	4.77	3.734	5.295	5.559	6.187	3.4
Cytotoxic T cell	2.905	4.306	0	3.932	4.548	3.782	2.856	4.092	3.024	2.283
CD3 T-cell	3.788	5.089	0	4.823	5.293	5.2	3.382	4.521	4.129	3.748
Double positive T cell	1.462	3.557	0	2.708	4.257	2.942	0.954	3.092	0.778	0.903
Exhausted T cell	3.098	4.952	0	4.352	5.347	4.1	2.71	4.43	3.019	2.279
Exhausted regulatory T cell	1.919	3.982	0	3.252	4.341	2.719	1.398	3.418	0.778	0.954
Helper T cell	3.533	5.285	0	4.793	5.571	5.254	2.893	4.536	3.465	3.296
Immunosuppressing carcinoma cell	3.722	3.876	1.146	3.725	3.918	1.908	5.64	5.556	3.773	1.301
Immunosuppressive B cell	0.954	2.146	0	1.204	3.976	1.255	2.538	3.588	0.845	0
Immunosuppressive T cell	2.201	3.838	0	3.157	4.905	3.525	3.745	4.875	1.544	1.415
Immunosuppressive macrophage Type 1	3.82	3.838	0	2.918	4.529	2.671	3.96	5.037	2.633	3.594
Immunosuppressive macrophage Type 2	3.896	3.893	0	2.59	4.734	2.569	3.726	5.075	2.297	3.098
Immunosuppressive natural killer cell	1.146	1.531	0	0.778	2.799	0.699	3.359	3.646	0.845	0.301
Macrophage Type 1	4.944	5.033	0.602	4.246	5.097	4.357	3.716	4.866	4.33	5.014
Macrophage Type 2	4.76	4.975	0.778	4.045	5.223	4.357	3.457	4.761	4.012	4.436
Natural killer cell	3.835	3.99	0	3.523	4.354	3.039	3.083	3.819	3.71	2.841
Regulatory T cell	2.663	4.474	0	3.81	4.956	4.194	2.526	4.198	2.33	2.467

Supplementary Table 4: LUAD cell counts per niche, displayed on a logarithmic scale (base 10) across the entire cohort. Each row represents a cell phenotype type and each column represents a niche, with color intensity indicating relative abundance. The use of a logarithmic scale highlights proportional differences in cell distribution.

	1	2	3	4	5	6	7	8	9	10
Activated cytotoxic T cell	4.23	3.04	4.24	0	2.15	2.74	4.31	0.3	0	1.3
Activated natural killer cell	2.72	2.25	2.78	0	1.26	1.73	3.06	0.3	0	1.28
B cell	3.92	3.35	4.17	2.19	3.77	2.85	5.13	2.44	1.89	2.87
CD8+ T cell	4.16	3.29	4.38	0	3.54	2.87	5.11	2.68	0.78	2.29
Carcinoma cell	6.09	6.22	5.37	6.29	3.57	5.52	4.71	2.35	2.12	3.52
Cytotoxic T cell	4.06	3.31	4.13	0	3.45	2.9	4.47	2.83	0.3	2.3
CD3 T-cell	4.64	4.1	4.44	2.66	4.76	3.37	5.24	4.34	2.39	3.6
Double positive T cell	2.63	1.18	3.03	0	2.48	1.08	3.93	0	0	0.6
Exhausted T cell	4.5	3.47	4.55	0	3.84	2.93	5.23	2.15	0.48	2.25
Exhausted regulatory T cell	3.7	2.07	3.79	0	2.65	1.9	4.34	0	0	1.32
Helper T cell	4.56	3.47	4.44	0	4.92	3	5.35	3.01	1.34	3.21
Immunosuppressing carcinoma cell	4.26	4.03	5.5	2.91	1.59	5.97	3.1	0	0	1.84
Immunosuppressive B cell	1.81	1	3.67	0	0.78	3.03	3.41	0	0	0.95
Immunosuppressive T cell	3.36	2.05	4.74	0	3.23	3.95	4.5	1.62	0	1.84
Immunosuppressive macrophage Type 1	4.03	3.36	4.82	0	2.52	4.27	4.32	0.6	0.48	3.84
Immunosuppressive macrophage Type 2	4.04	3.07	4.82	0	2.46	3.94	4.53	0	2.29	3.5
Immunosuppressive natural killer cell	1.57	1.11	3.48	0	0.95	3.46	2.46	0	0	0.85
Macrophage Type 1	4.84	4.59	4.67	2.18	4.09	3.95	5.03	2.74	2.03	4.87
Macrophage Type 2	4.78	4.27	4.64	2.58	4.26	3.71	5.15	2.67	4.05	4.41
Natural killer cell	3.86	3.64	4.06	1.87	3.07	3.08	4.15	2.19	2.05	2.97
Regulatory T cell	4.03	2.7	4.38	0	4.07	2.85	4.88	2.73	0.48	2.57
Regulatory T cell	2.66	4.47	0	3.81	4.96	4.19	2.53	4.2	2.33	2.47

Supplementary Table 5: LUSC cell counts per niche, displayed on a logarithmic scale (base 10) across the entire cohort.

Each row represents a cell phenotype type and each column represents a niche, with color intensity indicating relative abundance.

The use of a logarithmic scale highlights proportional differences in cell distribution.